DOI: https://doi.org/10.17816/gc655664 EDN: SVTGRR

Липополисахарид-индуцированное депрессивно-подобное состояние и нейровоспаление: дифференциальное влияние на гиппокамп и префронтальную кору у диких мышей

А.У. Исмаилова, К.В. Ичеткина, М.Р. Шульц, А.С. Шульц, Е.А. Курилова, О.П. Тучина

Балтийский федеральный университет имени Иммануила Канта, Калининград, Россия

АННОТАЦИЯ

Обоснование. Введение липополисахарида (LPS) мышам является широко используемой моделью для изучения депрессии, ассоциированной с воспалением. Однако механизмы, лежащие в основе вызываемых LPS изменений в мозге, остаются недостаточно изученными.

Цель. Целью данного исследования было изучение поведенческих, клеточных и молекулярных изменений, индуцированных интервальным введением LPS, в двух ключевых для патогенеза депрессии областях мозга — гиппокампе и префронтальной коре.

Методы. Исследование проведено на взрослых самцах диких мышей (n=28, возраст 2–3 мес, масса тела 25–35 г), а также на первичных культурах глиальных клеток.

Дизайн эксперимента включал введение LPS в дозе 1 мг/кг (3 инъекции внутрибрюшинно) в два этапа с 7-дневным интервалом. На первом этапе эксперимента оценивали поведенческие показатели, на втором проводили забор тканей (префронтальная кора и целый гиппокамп) для молекулярного и гистологического анализа. Для оценки поведения использовали тест «Открытое поле» (общая активность и тревожность), тест подвешивания за хвост, тест предпочтения сахарозы (ангедония) и Y-образный лабиринт (пространственная рабочая память). Первичные культуры клеток глии инкубировали в присутствии LPS — для индуцирования нейровоспаления и фактора роста фибробластов 2 (fibroblast growth factor, FGF2) — для оценки изменения фенотипа микроглиальных клеток.

Молекулярные и клеточные изменения *in vivo* и *in vitro* анализировали с помощью полимеразной цепной реакции в режиме реального времени и методов иммуногистохимии.

Результаты. Введение LPS вызвало у мышей депрессивно-подобное поведение, включая снижение интереса к гедоническому стимулу, увеличение времени нахождения в неподвижном состоянии, снижение общей двигательной активности и нарушения памяти. Воспалительная реакция сопровождалась повышенной экспрессией провоспалительных цитокинов (TNF-α, IL-1β) в селезёнке и головном мозге, при этом выявлены региональные различия в активации астроцитов и микроглии. У мышей, получавших LPS, наблюдали увеличение экспрессии белка плотных контактов 1 (tight junction protein 1, TJP1), фактора роста эндотелия сосудов A и E-селектина, снижение экспрессии клаудина 3, окклюдина, FGF2 и значительное повышение количества тучных клеток. В обоих отделах мозга отмечалась активация микроглии, сопровождающаяся увеличением доли амёбоидных форм клеток. В гиппокампе выявлены изменения глутаматергической передачи, включая снижение экспрессии глутаматного транспортера GLT-1 и глутаминсинтетазы, что указывает на нарушение механизмов буферизации глутамата. В экспериментах *in vitro* LPS индуцировал активацию микроглии, которая была нивелирована добавлением FGF2.

Заключение. Нейровоспаление, вызванное введением LPS, по-разному повлияло на гиппокамп и префронтальную кору, при этом гиппокамп демонстрировал бóльшую уязвимость. Обнаруженный нейропротекторный эффект FGF2 в отношении LPS-индуцированной активации микроглии указывает на его потенциальную роль в терапии депрессии, ассоциированной с воспалением.

Ключевые слова: липополисахарид; микроглия; астроциты; цитокины; глутамат; депрессия.

Как цитировать:
Исмаилова А.У., Ичеткина К.В., Шульц М.Р., Шульц А.С., Курилова Е.А., Тучина О.П. Липополисахарид-индуцированное депрессивно-подобное состояние и нейровоспаление: дифференциальное влияние на гиппокамп и префронтальную кору у диких мышей // Гены и клетки. 2025. Т. 20, № 3. С. 218–240. DOI: 10.17816/gc655664 EDN: SVTGRR

Рукопись получена: 12.02.2025 **Рукопись одобрена:** 08.07.2025 **Опубликована online:** 03.09.2025

Статья доступна по лицензии CC BY-NC-ND 4.0 International
© Эко-Вектор, 2025

DOI: https://doi.org/10.17816/gc655664 EDN: SVTGRR

Lipopolysaccharide-Induced Depressive-Like State and Neuroinflammatory Responses: Differential Effects on Hippocampus and Prefrontal Cortex in Wild-Type Mice

Ainazik U. Ismailova, Ksenia V. Ichetkina, Margarita R. Shults, Anton S. Shults, Ekaterina A. Kurilova, Oksana P. Tuchina

Immanuel Kant Baltic Federal University, Kaliningrad, Russia

ABSTRACT

BACKGROUND: Lipopolysaccharide (LPS) administration in mice is a widely used model for studying inflammation-associated depression. However, the mechanisms underlying LPS-induced changes in the brain remain unclear.

AIM: This study is aimed to investigate behavioral, cellular, and molecular changes induced by chronic-interval LPS treatment in two brain regions implicated in depression, the hippocampus and the prefrontal cortex.

METHODS: The study involved adult wild-type male mice (2–3 months old, 25–35 g, *n* = 28) and glial cell primary cultures. The experimental design included a two-phase LPS administration protocol (1 mg/kg, 3 injections intraperitoneally) with a 7-day interval. During the first phase, behavioral assessments were performed; whereas in the second phase, tissue samples (prefrontal cortex and whole hippocampus) were collected for molecular and histological analyses. Behavioral assessment included the Open Field Test (general activity and anxiety-like behavior), the Tail Suspension Test, the Sucrose Preference Test (anhedonia), and the Y-Maze Test (spatial working memory). Glial cell primary cultures were incubated in the presence of LPS to induce neuroinflammation and fibroblast growth factor 2 (FGF2) to assess changes in the microglial phenotype.
Molecular and cellular changes *in vivo* and *in vitro* were analyzed using real-time polymerase chain reaction and immunohistochemistry assays.

RESULTS: LPS-treated mice exhibited depression-like behavior, including decreased interest in hedonic stimulus, increased immobility, reduced locomotor activity, and memory deficits. The inflammatory reaction was associated with the elevated expression of proinflammatory cytokines (TNF-α, IL-1β) in both the spleen and brain with distinct regional patterns of astrocytic and microglial activation. LPS increased the expression of tight junction protein 1 (TJP1), vascular endothelial growth factor A (VEGFA), and E-selectin, decreased the expression of claudin 3, occludin, FGF2, and significantly increased the number of mast cells. Microglial activation was observed in both regions with a shift towards the amoeboid phenotype. Glutamatergic signaling was altered with downregulation of glutamate transporters (GLT-1) and glutamine synthetase in the hippocampus, suggesting the impaired glutamate buffering. *In vitro*, LPS induced microglial activation, which was reversed by FGF2.

CONCLUSION: LPS-induced neuroinflammation differentially affected the hippocampus and prefrontal cortex with the hippocampus appearing to be more vulnerable. FGF2 reversed LPS-induced microglial activation, indicating its potential as a therapeutic target for neuroinflammation-associated depression.

Keywords: lipopolysaccharides; microglia; astrocytes; cytokines; glutamic acid; depression.

To cite this article:
Ismailova AU, Ichetkina KV, Shults MR, Shults AS, Kurilova EA, Tuchina OP. Lipopolysaccharide-Induced Depressive-Like State and Neuroinflammatory Responses: Differential Effects on Hippocampus and Prefrontal Cortex in Wild-Type Mice *Genes & cells.* 2025;20(3):218–240. DOI: 10.17816/gc655664 EDN: SVTGRR

Submitted: 12.02.2025 **Accepted:** 08.07.2025 **Published online:** 03.09.2025

ECO•VECTOR

Article can be used under the CC BY-NC-ND 4.0 International License
© Eco-Vector, 2025

INTRODUCTION

In the 1980s, Zabrodskii first demonstrated that injections of armin (acetylcholinesterase inhibitor) decreased mice mortality rate in a model of experimental peritonitis caused by *Escherichia coli* [1]. Since then, our understanding of neuro-immune interactions has been significantly revised and further research of the mechanisms underlying the development of septic shock led to the discovery of a qualitatively new type of such interactions, the cholinergic anti-inflammatory pathway involving the vagus nerve [2]. Thus, the brain can control the development of the immune response. In turn, the immune system affects brain function and administration of lipopolysaccharide (LPS), a component of the gram-negative bacteria cell wall, is often used to study the mechanisms of inflammation-associated depression in different mouse strains [3]. Depression is one of the leading causes of mental disability worldwide [4] and inflammation is considered an important factor that worsens the course of the disease [5]. Whole transcriptome RNA sequencing revealed that several genes involved in immune regulation, cytokines and angiogenesis are downregulated in the brain of patients with depression [6]; thus, anti-inflammatory agents may have perspectives as future antidepressant treatments.

LPS-induced sickness behavior in mice include lower locomotor activity (as measured by the Open Field Test [OFT]), lower appetite, weight loss, and changes in body temperature, respiration rate, and sleep patterns. Depressive-like state is characterized by despair-like inhibitory learning behaviors (Tail Suspension Test [TST]), anhedonia (Sucrose Preference Test [SPT]) and memory deficits (Novel Object Recognition Task, Morris Water Maze, and Barnes Maze). It is well-known that LPS does not penetrate the blood-brain barrier (BBB) well and only 0.025% of LPS administered intravenously enters the rodent brain [7]. It is assumed that the main mechanisms of immune signal transmission from the blood to the brain include [8]:

1. Penetration of immune mediators directly from blood plasma to the brain through the areas where the BBB is leaky (choroid plexuses, circumventricular organs);
2. Activation of cytokine receptors on endothelial cells with subsequent formation of second messengers in the nervous tissue (e.g. prostaglandins E);
3. Active transport of immune mediators, such as tumor necrosis factor alpha (TNF-α) and interleukins. TNF-α is an early mediator of inflammation, the main source of which during the development of a systemic immune response is tissue macrophages, i.e. brain microglia.

Thus, inflammation-associated depression is most likely mediated by glial cells and, to some extent, by peripheral immune cells and their mediators. LPS may not penetrate the BBB but it triggers cellular and molecular changes in the brain. According to recent studies, depressive disorder affects many brain regions, including the prefrontal cortex (PFC), anterior cingulate cortex, amygdala, hippocampus, cerebellum, and the basal ganglia [9] and chronic stress-induced depression is associated with neuroinflammation and altered glutamate signaling [10]. As the exact mechanisms underlying LPS-induced depressive-like state are unknown, we have decided to investigate the cellular and molecular changes in response to LPS in two brain regions implicated in depression, including the PFC and the hippocampus, using complex approach, from behavior phenotyping of LPS-treated mice to polymerase chain reaction (PCR) assays, histology, and cell culture experiments.

AIM

This study aimed to investigate the behavioral, cellular, and molecular changes induced by chronic-interval LPS administration in two brain regions implicated in depression—the hippocampus and the PFC. By employing behavioral tests, histological analyses, real-time PCR, and glial cell primary culture experiments, we sought to identify region-specific neuroinflammatory responses and glutamatergic signaling alterations.

METHODS

Animals and Lipopolysaccharide Injection Protocol

Adult male wild-type (house) mice were purchased from a breeder of fancy mice (for subsequent sale to pet stores or individuals) and kept in the university animal facility. Mice (2–3 months old, 25–35 g, n = 28) were randomized into control or LPS-treated groups across three experimental cohorts: 5/5 (Control/LPS) in cohort 1, 5/4 in cohort 2, and 4/5 in cohort 3. Different subsets of animals were used in different experiments (behavioral testing, gene expression analysis, histology analyses, and immunohistochemistry assays); sample sizes may vary between figures due to the nature of each experiment and subsequent technical limitations. In several cases, animals were excluded from specific analyses *post hoc* due to technical issues. Detailed group sizes used in each experiment and reasons for exclusion are provided in Supplement 1. All animals were housed 4–5 per cage and kept in standard environmental conditions (23 ± 2 °C; 12 h / 12 h dark/light cycle) with water and food provided *ad libitum* in the animal care facility at Immanuel Kant Baltic Federal University (IKBFU) in Kaliningrad, Russia. All experiments, including the number of animals used in the study, were approved by the Independent Ethical Committee of the Clinical Research Center at IKBFU, Kaliningrad (protocol No. 27/2024). Animals were randomized into the control and LPS-treated groups. LPS (1 mg/kg, L2880; Sigma-Aldrich, USA) was dissolved in saline solution (0.9% NaCl). Two phases of injections (3 intraperitoneal injections per phase) were administered with a 7-day interval. Mice

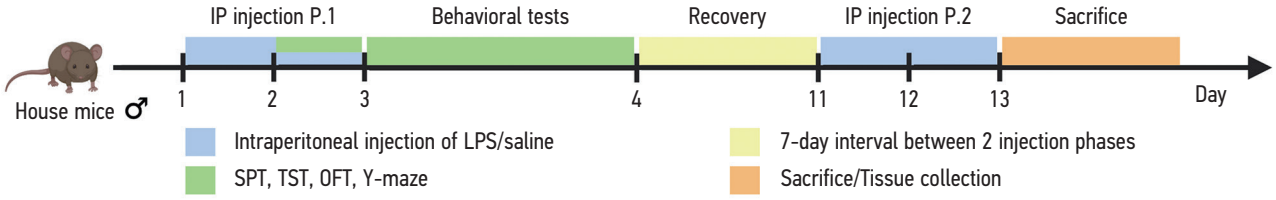

Рис. 1. Дизайн эксперимента. SPT — тест предпочтения сахарозы, TST — тест подвешивания за хвост, OFT — тест «Открытое поле», Y-maze — Y-образный лабиринт. IP injections — интраперитонеальные инъекции липополисахарида/раствора хлорида натрия.
Fig. 1. Study design. SPT, Sucrose Preference Test; TST, Tail Suspension Test; OFT, Open Field Test; Y-maze, Y-maze test. IP injection, intraperitoneal injections of lipopolysaccharide/saline.

were intraperitoneally (i.p.) injected with LPS or sterile saline trice for behavior tests (phase 1) and trice for brain dissection and gene expression analysis (phase 2). Mice body weight was measured at days 1 and 3 of the injection. Experimental design is shown in Fig. 1.

Behavior Phenotyping

At day 3, 4 hours after the third i.p. injection, the animals were screened using behavior tests as follows: OFT, TST, Y-Maze Test. The SPT was performed after the second i.p. injection due to its 24-hour duration. Before the behavioral tests (at least 30 minutes in advance), the cages with mice were placed in the behavioral testing facility for the animals to get used to the new environment. All mazes were first wiped with a damp cloth and then with a 70% ethanol wipe; the room was ventilated between tests for at least 5 minutes. Mice activity was recorded with a GoPro HERO9 Black camera and the behavior was analyzed using BehaviorCloud (Columbus, USA).

Open Field Test

To test exploratory behavior and general activity in the OFT, mice were individually placed into the corner of an open arena (50 × 50 × 60 cm) with dim lighting and allowed to move freely for 5 minutes. In the OFT, the time spent by the animal in the center and at the periphery of the maze was assessed. In addition, we considered how many times the mice crossed the center, how much time they spent moving, and the number of supported rears.

Tail Suspension Test

The TST was performed to assess depression-like behavior, such as behavioral despair, and learned helplessness. The test facility consisted of 4 chambers, where mice were suspended (at a height of 50 cm from the floor) by their tails using sticky tape at 1 cm from its tip. Each mouse was kept in a separate chamber in moderately bright lighting (300 Lux) conditions without the possibility of visual or tactile contact with the surrounding area and other animals. The TST was conducted for 5 minutes, the immobilization time and latency period were recorded. Slight movements of front paws without hind paws were not considered as mobility. TST data were analyzed manually using stopwatch.

Sucrose Preference Test

The SPT was performed to assess anhedonia-like behavior. For the SPT, mice were habituated for 48 hours to two bottles filled with water or 2% sucrose solution at their home cages before the injections. During the test, mice were kept alone in their home cage without food restrictions. After the second injection (phase 1), two bottles with 100 mL of water or 2% sucrose solution were placed in each cage. The position of the sucrose-containing bottle was balanced across cages and groups. After 24 hours, the weight of the remaining liquid in both bottles was measured. Thus, the total time from habituation to sucrose to the end of the test was 72 hours. The sucrose preference was calculated using the following formula: preference = (sucrose intake (mL) / total liquid intake (mL)) × 100%.

Y-Maze Test

Y-maze test was used to evaluate the short-term spatial working memory and exploratory activity of mice. The test is performed in a Y-shaped maze with three opaque arms (33 × 9 × 15 cm) separated equally at 120°. Visual cues in black and white were placed on the proximal part of each arm and designated as zones A, B, and C. Additionally, on the distal part, the same signs were duplicated in larger sizes on the indicators. The test was performed under dim lighting (150 Lux). The Y-maze test consisted of two phases (a learning phase and a training phase) with an intertrial interval of 1 hour. During the learning phase, one arm was closed with the divider (designated as new). Each mouse was placed into one open arm facing the center, allowing it to explore the maze for 10 minutes, then the test mouse returned to the home cage. After 1 hour, the divider was removed and the training phase was conducted to test spatial memory. The mouse was placed into the same arm as in the learning phase and allowed to explore the maze for 5 minutes. For the analysis, we considered the number of entries into the new arm, time spent exploring the new arm, and spontaneous alternation (as percentage alternation). Arm entries were counted when the mouse's hind paws were inside the sleeve area. Spontaneous alternation is known as consecutive entries into each arm of the maze without repetitions calculated by the following formula: [% alternation = number of alteration / total arm visits — 2],

where the lower percentage of spontaneous alternation is considered memory impairment.

Brain Dissection

Four hours after the third i.p. injection (phase 2), the animals were deeply anesthetized with isoflurane (Aesica Queenborough, UK), transcardially perfused, and decapitated. The anesthetic was used in accordance with the safety instructions for working with volatile substances; therefore, the mice were anesthesized in a desiccator with a fume hood. The mice were decapitated after checking the effect of anesthesia (typical signs include loss of consciousness, muscle relaxation, pain insensibility, and slow, barely noticeable breathing). A 0.9% solution of sodium chloride was used to wash the cerebral vessels during perfusion. Brain isolation was performed in a clean room using medical instruments and a blood disinfectant. After dissection, the brain was cut into hemispheres; the hippocampus and PFC were isolated from one hemisphere for the subsequent PCR. The other hemisphere was fixed in 4% paraformaldehyde (PFA) in a sodium phosphate buffer (phosphate buffered saline [PBS], pH 7.4) for 48 hours at 4 °C. At least 24 hours before the preparation of serial brain slices, the hemispheres were placed in a 30% sucrose solution. Before preparing the slices, the cerebral hemisphere was carefully removed from sucrose solution, fixed on a cold plate using a freezing agent (KEDEE, China), and placed on a freezer shelf inside a Leica cryostat (Leica Microsystems, Germany). After freezing the brain, the cold plate was transferred from the freezer shelf to the sample holder and serial 50 µm frontal sections of the cerebral hemispheres were made. The slices were serially arranged in 6-well plates in PBS (phosphate-buffered saline) with Triton X-100 (PBST, 0.01%). Each of the six series was used for a different staining type. All sections in every series were examined, allowing the total coverage of the examined brain region.

Histology: Mast Cell Identification

For histology analyses, the cerebral hemispheres were stored in a 4% PFA solution at +4 °C. Next, the hemispheres were placed in a 30% sucrose solution for at least 24 hours to remove the remaining fixative from the tissues. Then, as described above, 50 µm frontal sections of the hemispheres were made using a Leica cryostat (Leica Microsystems, Germany). The slices were serially arranged in 6-well plates in PBS with Triton X-100 (PBST, 0.01%). Next, frontal rostral and caudal slices were placed on glass slides pretreated with gelatin. To identify mast cells, glass slides with slices were placed in 10% brilliant green for 60 seconds, then washed with running water and placed in 1% methylene blue for 15 seconds. Then the slides were washed with running water and placed in 98% ethyl alcohol for 15–20 seconds, then in xylene for 10–15 seconds. The slide with sections was treated with Eukitt® medium (Sigma-Aldrich, USA) and a cover glass was installed. Mast cells were counted in whole brain and the hippocampal slices, including the perivascular spaces between the hippocampus and thalamus, using Leica DM4000B fluorescence microscopes (Leica Microsystems, Germany) and Zeiss Axio Imager.A2 with Axiocam 506 digital camera (Zeiss, Germany).

Immunohistochemistry Assays

For immunohistochemistry assays, one hemisphere was stored in a 4% PFA solution at 4 °C, then placed in 30% sucrose solution for at least 24 hours for cryoprotection before brain dissection. The resulting serial 50 µm slices were arranged on 6-well plates with Triton X-100 PBS (PBST, 0.01%) and stored in PBS + 0,01% NaN3 to prevent pathogen growth. Brain sections were washed trice in PBS for 10 minutes and treated with 5% bovine serum albumin (BSA, batch: 68100/BB20561101; PanEco, Russia), in PBS with 0.03% Triton X-100 (2725C289; Sigma-Aldrich, USA) overnight at 4 °C. For immunostaining, sections were incubated for 48 hours at 4 °C with the primary antibodies, including rabbit polyclonal Iba1 (Affinity Biosciences, China, DF7217; 1:1000), mouse monoclonal GFAP (2E1) (Santa Cruz Biotechnology, USA, sc-33673; 1:1000), rabbit polyclonal EAAT2 (GLT-1) (Abcam, UK, ab41621; 1:1000) antibodies, diluted in 1% BSA. After incubation with primary antibodies, sections were washed thrice in PBS for 10 minutes and incubated with secondary antibodies, including donkey anti-rabbit Alexa Fluor 488 (Abcam, UK, ab150073; 1:1000) or goat anti-mouse-Cy3 (Cusabio, China, L0117G; 1:1000) overnight at 4 °C. After the three washes with PBS, sections were arranged on glass slides with a mowiol-based mounting medium. Images were taken on a fluorescent microscope Leica DM4000B (Leica Microsystems, Germany) and the corrected total cell fluorescence (CTCF) was analyzed using Fiji (ImageJ 1.53t) by the following formula: Integrated density (sum of pixel intensities of all object pixels)—(cell area × mean fluorescence of background readings). The number of microglia was determined by manual counting using the fluorescent microscope Leica DM4000B. Z-stack images were taken at 6.11 µm intervals over a 50 µm Z-range using an inverted Zeiss LSM 700 laser scanning confocal microscope to analyze microglial area and morphology. For each animal, three frontal sections were selected for both the hippocampus and the medial PFC (mPFC), corresponding to the rostral, middle, and caudal parts of these structures. Sections were selected based on anatomical landmarks identified using the Allen Brain Atlas. In the hippocampus, the anterior section was made at the point where the hippocampus first becomes visible; the middle section corresponded to a region with well-defined layers of the dentate gyrus and hippocampal cornu ammonis (CA) subfields, and the posterior section was made where the dentate gyrus appears elongated and curved. In the mPFC, sections were chosen to represent rostral, middle, and caudal parts of the cingulate, prelimbic, and infralimbic areas. For each selected section, confocal images were taken and 15 microglial cells were randomly selected per animal for analysis using Fiji software. Thus, 450 microglial cells were

examined in the hippocampus and 450 cells in the mPFC in the control group (n = 10 animals) and 405 cells per the respective region in the experimental group (n = 9 animals).

In Z projection images, 3 microglial phenotypes were analyzed, including the ramified microglia with small cell body and highly arborized branches, intermediate microglia with enlarged/elongated soma and retracted branches, and ameboid microglia with swollen rounded cell body with few or no branches.

Cell Culture Experiments

Primary mixed glial cultures were obtained under modernized protocols [11–13] from the hippocampus of postnatal day 3 (P3) neonatal mice. The experimental animals were euthanized by rapid decapitation. The brain was extracted using sterile forceps and the hippocampus was dissected. The obtained tissue was dissociated using TrypLE (Thermo Fisher Scientific, USA). Cell suspensions were seeded onto coverslips covered with poly-D-lysine at a seeding density of 4.5×10^5 cells/cm^2 in 6-well plates. The plates were then placed in a CO_2 incubator and cultured under standard conditions at 37 °C, 95% humidity, and 5% CO_2 for 8 days. The culture medium consisted of 87.9% Dulbecco's Modified Eagle Medium (DMEM) with high glucose (Thermo Fisher Scientific, USA) content and 10% fetal bovine serum (Thermo Fisher Scientific, USA). Additionally, 1X with L-glutamine (Thermo Fisher Scientific, USA), 100 U/mL / 100 µg/mL Penicillin-Streptomycin solution (Thermo Fisher Scientific, USA), and 0.25 µg/mL amphotericin B (Thermo Fisher Scientific, USA) were added. When the cell cultures in the experimental groups reached 80% confluence, 200 ng/mL recombinant human FGF2 derived from *E. coli* (abm, Canada) was added to the culture medium. To build a model of induced neuroinflammation, 100 ng/mL bacterial LPS from *E. coli* (Sigma-Aldrich, USA) was introduced into the culture medium. To evaluate the individual and combined effects of these agents, cells were incubated for 6 or 12 hours across eight experimental groups, including the control 6/12 hours (cultured in medium without LPS and FGF2), LPS 6/12 hours, FGF2 6/12 hours, and LPS + FGF2 6/12 hours.

Immunocytochemistry Assays

To perform immunocytochemical staining, the cell monolayer was pre-washed thrice with Dulbecco's Phosphate-Buffered Saline (DPBS) containing calcium and magnesium (Thermo Fisher Scientific, USA) and fixed with a 4% PFA solution for 20 minutes. Cells were then washed thrice with PBS with 0.1% Tween 20 for 5 minutes each. To block nonspecific antibody binding, a 1% BSA solution in PBST was applied for 1 hour. Next, the cells were sequentially incubated with primary monoclonal antibodies, rabbit Iba-1 (ab178847, 1:1000; Abcam, UK) and goat GFAP (ab53554, 1:2000; Abcam, UK) at +4 °C for 48 hours. Then, secondary polyclonal antibodies conjugated to fluorescent labels were used, donkey anti-rabbit IgG labeled with Alexa Fluor® 488 (ab150073; Abcam, UK) and donkey anti-goat IgG labeled with Alexa Fluor® 555 (ab150130; Abcam, UK) for 24 hours at ambient temperature. Cytological preparations were mounted using Fluoroshield™ medium with diamidinophenylindole (DAPI) for nuclear staining (Sigma-Aldrich, USA). Digital images of the samples were taken using a fluorescent microscope (Axio Imager.A2; Carl Zeiss, Germany) with a ZEISS Axiocam 506 digital camera (Carl Zeiss, Germany) and a 20x EC Plan Neofluar objective. Images were processed using the special software ZEN Pro. Fluorescent labels Alexa Fluor® 488 and Alexa Fluor® 555, as well as DAPI-labeled nuclei, were excited using lasers with wavelengths of 355 nm, 488 nm, and 555 nm, respectively. Iba-1+ cells, cell microglial area, and the ratio of microglial phenotypes were measured using Fiji (ImageJ 1.53t). Cell phenotypes and microglial areas were analyzed in 10 randomly selected fields of view in each image for a total of 100 cells.

Real-Time Polymerase Chain Reaction

The hippocampus, the PFC, and the spleen were isolated from the mice and homogenized with plastic pestles. The ExtractRNA agent (Evrogen, Russia) was used for total RNA extraction using phenol-chloroform extraction method; the amount of RNA was measured using NanoPhotometer Pearl (Implen, Germany) and complementary DNA (cDNA) was synthesized using MMLV RT Kit (Evrogen, Russia) according to the manufacturer's protocol. The amount of isolated RNA was measured based on the absorbance ratio of 260/230 (samples with a ratio of approx. 2.0 were used in the study). To assess the purity, we performed real-time PCR assays, where the isolated RNA was used as a matrix for synthesis. If the curves did not rise, the sample was clean of genomic DNA. We designed primers using NCBI Primer-BLAST software (http://www.ncbi.nlm.nih.gov/tools/primer-blast/) and selected primer pairs with the least probability of amplifying nonspecific products as predicted by NCBI Primer-BLAST. The real-time PCR primers used in this study are listed in Supplement 2. Gradient qPCR was done to optimize the primers. The specificity of amplification was assessed using melting curves (Supplement 3) and electrophoresis (Supplement 4). The qPCR assay was performed with 5X qPCRmix-HS SYBR (Evrogen, Russia) using a CFX96 Real-Time System (Bio-Rad, USA) under the following conditions:

a. 3 minutes at 95 °C followed by 39 cycles at 95 °C for 15 seconds and 63 °C/57 °C for 35 seconds;
b. 2 minutes at 50 °C followed by 95 °C for 5 minutes and 39 cycles at 95 °C for 15 seconds and 63 °C for 35 seconds.

A melting curve of amplified products was determined after qPCR. The gene expression was quantified by comparison with a standard curve and normalized relative to reference genes (β-actin, GAPDH). Data were collected using CFX Manager 3.1 (Bio-Rad, USA) and analyzed by Delta-Delta Ct method.

Statistical Analysis

GraphPad Prism 8 (GraphPad, USA) was used for statistical analysis and graphing. The Shapiro–Wilk test was used to determine the normality of the variables and unpaired *t*-test was used to compare two separate groups with equal variance. For non-normally distributed data, Mann–Whitney U test was used. Statistical differences for two independent variables between groups were determined using the two-way analysis of variance (ANOVA) with repeated measurements followed by Tukey's honestly significant difference test. Significance levels are indicated as * $p \leqslant 0.05$, ** $p \leqslant 0.01$, *** $p \leqslant 0.001$, **** $p \leqslant 0.0001$.

RESULTS

Chronic-Interval lipopolysaccharide Treatment Induced Depressive-Like Behaviors, Weight Loss, and Memory Deficits in Mice

After 3 days of LPS injections mice showed significant loss of body weight ($p = 0.0077$, see Fig. 2c). In addition, LPS injections affected mouse behavior in the OFT and TST (see Fig. 2b, d–f). After LPS treatment, mice spent significantly more time in the OFT field compared to its center ($p = 0.0046$), locomotor activity decreased ($p = 0.0021$), and we observed a lower total number of rears ($p = 0.0006$). Thus, their exploratory behavior substantially decreased. LPS-treated mice displayed depressive-like and/or sickness behaviors, including higher immobility in the TST ($p = 0.041$, see Fig. 2b) and lower sucrose preference in the SPT ($p = 0.0167$, see Fig. 2a). We assessed the short-term spatial working memory of LPS-treated mice by the Y-maze test. As shown in Fig. 2, g–i, LPS significantly decreased the spontaneous alternation ($p = 0.0008$) and the number of novel arm entries ($p = 0.0002$) compared with the control group. This shows that LPS injections promote anxiety-like and depressive-like behavior and memory and learning impairment in mice. The additional behavioral assessments are shown in Supplement 5.

Lipopolysaccharide Injections Promoted Expression of Proinflammatory Cytokines in the Spleen and Brain

LPS promoted changes in the expression of cytokines in the spleen (see Fig. 3a), the hippocampus (see Fig. 3b) and the PFC (see Fig. 3c). However, the expression patterns were different. We observed significant elevation of IL-1β and TNF-α expression in the spleen ($p = 0.0082$ and $p = 0.0049$) and both brain regions ($p < 0.0001$ and $p = 0.0395$ for the hippocampus; $p = 0.0002$ and $p < 0.002$ for the PFC); whereas IL-6 and IL-10 expression was elevated in the spleen ($p = 0.0285$ and $p = 0.0014$), lower in the hippocampus ($p = 0.0036$ and $p = 0.0151$), and did not change significantly in the PFC ($p = 0.1631$ and $p = 0.3710$) compared to control animals.

Expression Changes in BBB Markers, VEGFA, and FGF2 Induced by Chronic-Interval Lipopolysaccharide Treatment

We investigated the expression of vascular endothelial growth factor A (VEGFA), fibroblast growth factor 2 (FGF2) and endothelial-leukocyte adhesion molecule 1, or E-selectin/CD62E (see Fig. 4, a–c), and tight junction proteins TJP1/Zonula Occludens-1 (ZO-1), occludin, and claudin 3 (see Fig. 4, d–f) in the hippocampus and PFC in response to LPS injections. Post-LPS treatment expression of TJP1 increased significantly in both brain regions ($p = 0.0008$ for the hippocampus; $p = 0.0035$ for the PFC); whereas the expression of occludin and claudin 3 decreased ($p = 0.0176$ and $p = 0.0149$ for the hippocampus; $p = 0.0043$ and $p = 0.0057$ for the PFC). The expression of VEGFA ($p = 0.0025$ for the hippocampus; $p = 0.0002$ for the PFC) and E-selectin ($p < 0.0001$ for the hippocampus; $p < 0.0001$ for the PFC) increased significantly; whereas the level of FGF2 decreased, especially in the hippocampus ($p = 0.0019$ for the hippocampus; $p < 0.0001$ for the PFC), compared to control animals.

Chronic-Interval Lipopolysaccharide Treatment Resulted in an Increased Number of Mast Cells in the Brain

Intraperitoneal injection of LPS resulted in an increased number of resident mast cells in the mouse brain, especially in the perivascular areas between the hippocampus and thalamus. The mast cells were identified after brilliant green/methylene blue staining by their oval shape, size (20–25 μm), and numerous dark purple granules in the cytoplasm (see Fig. 5, a–d). The mast cells were localized in the perivascular spaces of the thalamus, cerebral cortex, and hippocampus. In addition, single cells were found in the parenchyma of the cerebral cortex and the dentate gyrus of the hippocampus (see Fig. 5a). Multiple cells, including the degranulating mast cells (see Fig. 5d), were localized in the vessels between the hippocampus and thalamus (see Fig. 5, b, c). LPS treatment resulted in a significant increase in the total number of mast cells in the brain ($p = 0.0192$, see Fig. 5e) and the hippocampal area ($p = 0.0067$, see Fig. 5f) compared to control mice. In addition, we observed a significant elevation of c-KIT tyrosine kinase receptor gene expression in the hippocampus ($p = 0.0030$, see Fig. 5g), a gene essential for mast cell survival, differentiation, and degranulation.

Chronic-Interval Lipopolysaccharide Treatment Resulted in Astrocytic and Microglial Activation and the Increased Number of Microglial Cells in the Hippocampus and Medial Prefrontal Cortex

To investigate the microglial and astrocytic activation in response to LPS administration, the mRNA expression of

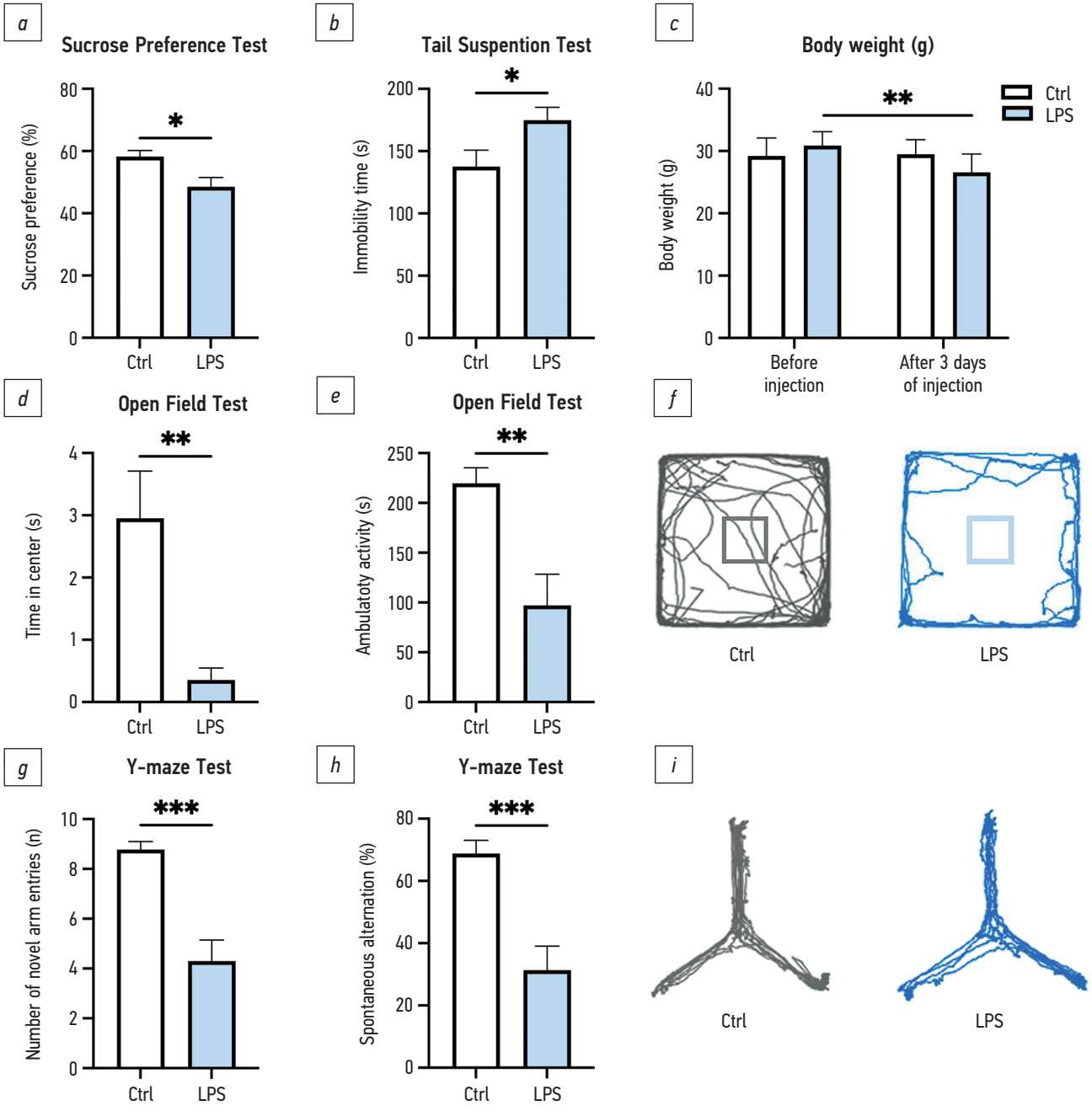

Рис. 2. Эффект введения LPS на поведение и массу тела мышей: *a* — предпочтение сахарозы в SPT, *b* — время неподвижности в TST, *c* — масса тела мышей после 3 дней инъекций, *d* — время в области центра OFT, *e* — двигательная активность в OFT, *f* — репрезентативные треки передвижения мышей в OFT, *g* — количество заходов в новый рукав в Y-maze тесте, *h* — спонтанное чередование в Y-maze тесте, *i* — репрезентативные треки передвижения мышей в Y-maze тесте. LPS — липополисахарид, Ctrl — контрольная группа; *n*=9/10 (Ctrl/LPS) для рис. *b*, *h*, *i*; *n*=10/9 (Ctrl/LPS) для рис. *c*–*f*. Данные представлены как средние ± SEM; * $p \leq 0{,}05$; ** $p \leq 0{,}01$; *** $p \leq 0{,}001$ (t-тест, тест Манна–Уитни, двухфакторный тест ANOVA).

Fig. 2. Effect of LPS treatment on mice behavior and body weight: *a*, sucrose preference in the SPT; *b*, immobility time in the TST; *c*, body weight of mice before and at 3 days of injections; *d*, time in the center in the OFT; *e*, ambulatory activity in the OFT; *f*, representative tracks of mice in the OFT; *g*, novel arm entries in the Y-maze test; *h*, spontaneous alternation in the Y-maze test; *i*, representative tracks of mice in the Y-maze test. LPS, lipopolysaccharide; Ctrl, control group; *n* = 9/10 (Ctrl/LPS) for *b*, *h*, *i*; *n* = 10/9 (Ctrl/LPS) for c–*f*. Data are presented as mean values ± SEM; * $p \leq 0.05$, ** $p \leq 0.01$, *** $p \leq 0.001$ (*t*-test, Mann–Whitney test, ANOVA).

Iba1 and glial fibrillar acid protein (GFAP) were analyzed (see Fig. 6e and Fig. 7b). Expression of the microglial marker Iba1, ionized calcium-binding adaptor molecule 1, significantly decreased both in the hippocampus ($p = 0.0050$) and the PFC ($p = 0.0108$). Ramified, intermediate, and ameboid phenotypes of Iba1+ cells were quantified with 15 randomly selected fields using confocal microscopy of immunohistochemical images (see Fig. 6b). The morphological assessment of Iba1+ cells showed less than 6% of ameboid phenotype in both brain regions with more than 80% cells maintaining

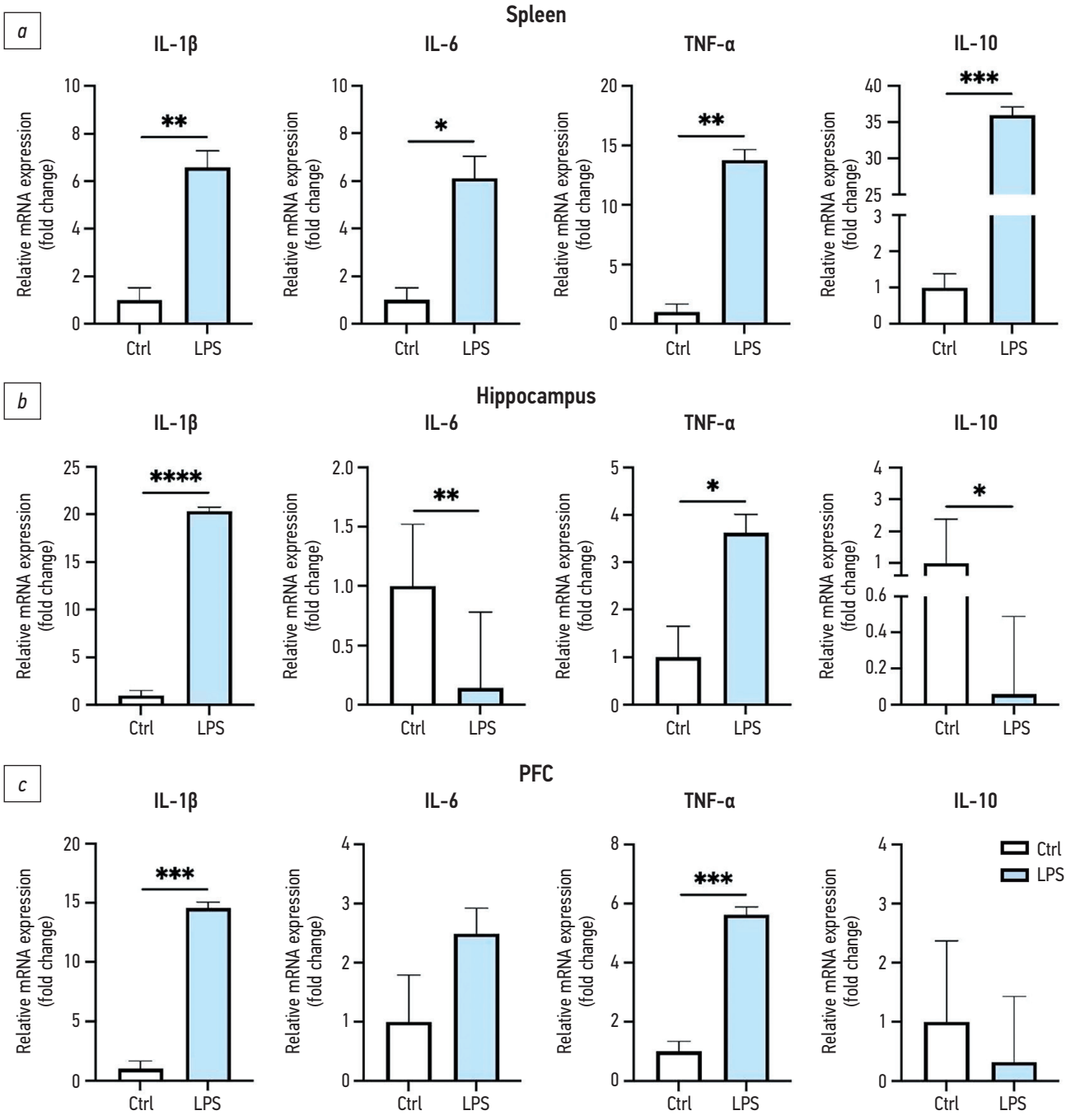

Рис. 3. Уровни экспрессии про- и противовоспалительных цитокинов в селезёнке, гиппокампе и префронтальной коре мышей в ответ на введение LPS: *a–c* — уровни экспрессии генов. LPS — липополисахарид, Ctrl — контрольная группа, TNF-α — фактор некроза опухоли α, IL — интерлейкины-1β, -6 и -10 соответственно, PFC — префронтальная кора, mRNA — матричная рибонуклеиновая кислота; *n*=7/7 (Ctrl/LPS) для рис. *a*; *n*=8/8 (Ctrl/LPS) для рис. *b*, *c*. Данные представлены как средние ± SEM; * $p \leqslant 0{,}05$; ** $p \leqslant 0{,}01$; *** $p \leqslant 0{,}001$; **** $p \leqslant 0{,}0001$ (t-тест).

Fig. 3. Expression of pro- and antiinflammatory cytokines in the spleen, hippocampus, and prefrontal cortex of mice in response to LPS treatment: *a–c*, gene expression levels. LPS, lipopolysaccharide; Ctrl, control group; TNF-α, tumor necrosis factor alpha; IL, interleukins 1β, 6 and 10, respectively; PFC, prefrontal cortex; mRNA, messenger ribonucleic acid; *n* = 7/7 (Ctrl/LPS) for *a*; *n* = 8/8 (Ctrl/LPS) for *b*, *c*. Data arepresented as mean values ± SEM; * $p \leqslant 0.05$, ** $p \leqslant 0.01$, *** $p \leqslant 0.001$, **** $p \leqslant 0.0001$ (*t*-test).

ramified morphology. However, in LPS-treated mice, more than 55% cells had intermediate morphology, more than 26% of LPS-treated mice microglia were ameboid, and less than 19% exhibited ramified morphology (see Fig. 6c). In addition to morphological analysis, we measured the microglial cell area and the total amount of Iba1+ cells. There was a significant increase in the microglial cell area compared with the control group (see Fig. 6d) as a result of induced neuroinflammation. The number of microglia was significantly higher after LPS injections in the molecular

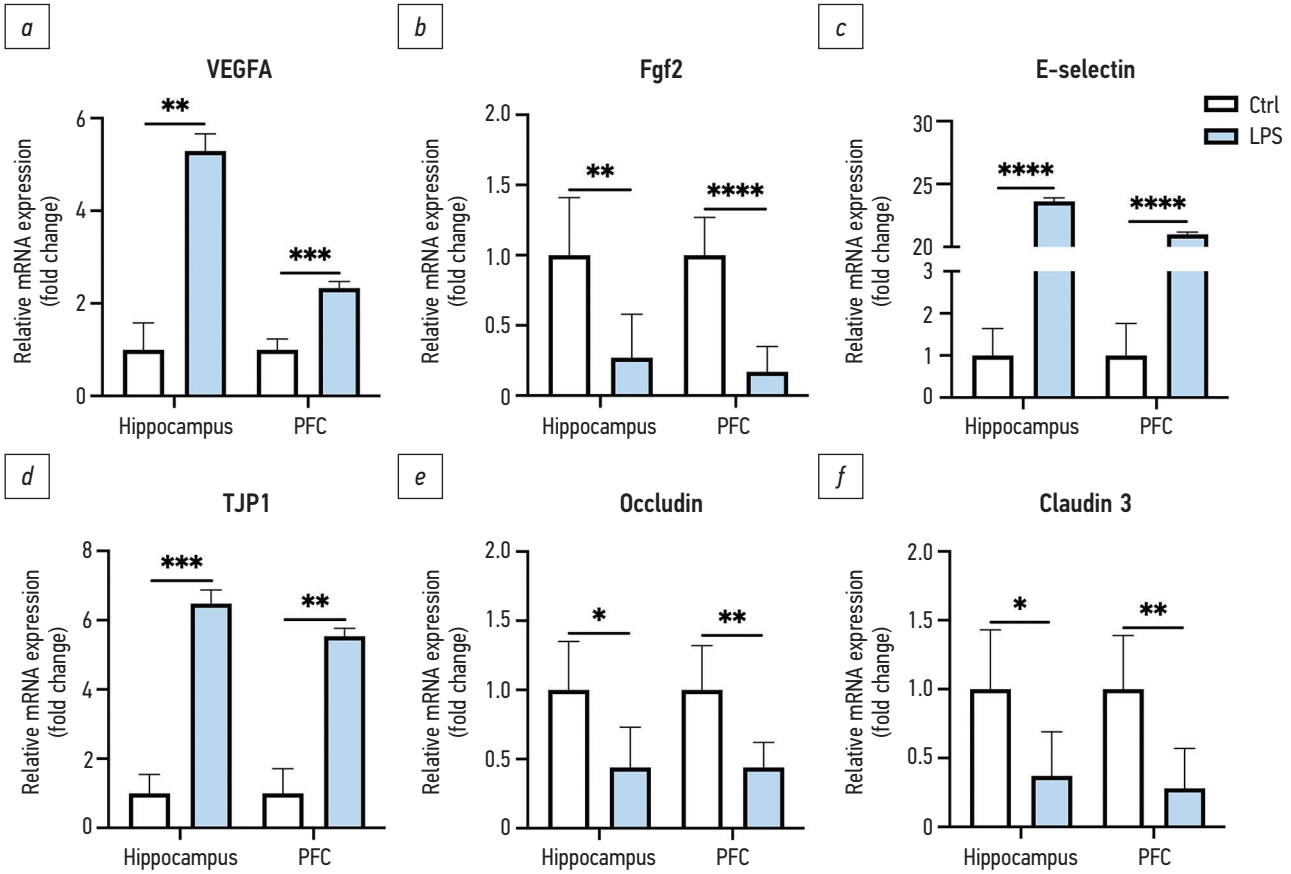

Рис. 4. Уровни экспрессии маркёров и регуляторов проницаемости ГЭБ в гиппокампе и префронтальной коре мышей в ответ на введение LPS: *a–f* — уровни экспрессии генов. LPS — липополисахарид, Ctrl — контрольная группа, VEGFA — фактор роста эндотелия сосудов A, FGF2 — фактор роста фибробластов 2, E-selectin — CD62-подобный антиген семейства E, молекула адгезии эндотелиальных лейкоцитов 1, TJP1/ZO1 — белок плотных контактов 1/zonula occludens-1, Occludin, Claudin 3 — трансмембранные белки плотных контактов, PFC— префронтальная кора (ПФК); для VEGFA, FGF2, Occludin и Claudin 3 *n*=9/10 (Ctrl/LPS), для E-selectin и TJP1 в ПФК *n*=8/10 и *n*=8/9 соответственно. Данные представлены как средние ± SEM; * $p \leqslant 0{,}05$; ** $p \leqslant 0{,}01$; *** $p \leqslant 0{,}001$; **** $p \leqslant 0{,}0001$ (t-тест, тест Манна–Уитни).

Fig. 4. Expression of markers and regulators of BBB permeability in the hippocampus and prefrontal cortex of mice in response to LPS treatment: *a–f*, gene expression level. LPS, lipopolysaccharide; Ctrl, control group; VEGFA, vascular endothelial growth factor A; FGF2, fibroblast growth factor 2; E-selectin, CD62 antigen-like family member E, endothelial-leukocyte adhesion molecule 1; TJP1/ZO1, tight junction protein 1/Zonula Occludens-1; Occludin, Claudin 3, tight junction transmembrane proteins; PFC, prefrontal cortex; *n* = 9/10 for VEGFA, FGF2, Occludin, and Claudin 3 (Ctrl/LPS), except for E-selectin and TJP1 in the PFC (*n* = 8/10 and *n* = 8/9, respectively). Data are presented as mean values ± SEM; * $p \leqslant 0.05$, ** $p \leqslant 0.01$, *** $p \leqslant 0.001$, **** $p \leqslant 0.0001$ (*t*-test, Mann–Whitney test).

layer (mlDG), granular layer (glDG), and hilus of the dentate gyrus (see Fig. 6f) compared to controls. We observed dense bundles of Iba1+ cells in the perivascular regions between the hippocampus and thalamus and the perivascular spaces in the mPFC of mice from the LPS group, which led us to count microglial cells in those areas (see Fig. 6, g, h). In addition, we analyzed CTCF of Iba1+ cells in the perivascular area between DG and CA1slm ($p < 0.0001$, see Fig. 6d). The increase in the amount of microglial cells was statistically significant in all analyzed regions of the LPS-treated mice ($p < 0.0001$ for all areas, see Fig. 6, f–h, j). Visually, there was a noticeable difference in the fluorescence intensity between the two groups (see Fig. 6a).

However, gene expression of GFAP, a glial fibrillary acidic protein known as an astrocyte marker, was significantly lower in the hippocampus ($p = 0.0101$) and higher in the PFC ($p = 0.0003$). We examined fluorescence intensity of astrocyte marker GFAP+ cells in the hippocampal and medial PFC regions in response to LPS treatment (see Fig. 7). The fluorescence intensity of GFAP+ cells was significantly higher after LPS injections in the molecular layer (mlDG), granular layer (glDG), hilus of the dentate gyrus and the mPFC area compared to controls ($p = 0.0005$ for mlDG; $p = 0.0008$ for glDG; $p = 0.0003$ for hilus; $p = 0.0053$ for mPFC; see Fig. 7, c, g). In addition, we observed a statistically significant increase in the fluorescence intensity of astrocyte marker GFAP+ cells in the perivascular regions between the hippocampus and thalamus and the perivascular spaces in the mPFC of mice from the LPS group ($p = 0.0002$ for Fig. 7d; $p < 0.0001$ for Fig. 7f). We also analyzed CTCF of GFAP+ cells in the perivascular area between DG and CA1slm ($p < 0.0001$, see Fig. 7e). Similar to Iba1 staining, GFAP staining demonstrated the increased fluorescence in the analyzed regions (see Fig. 7a).

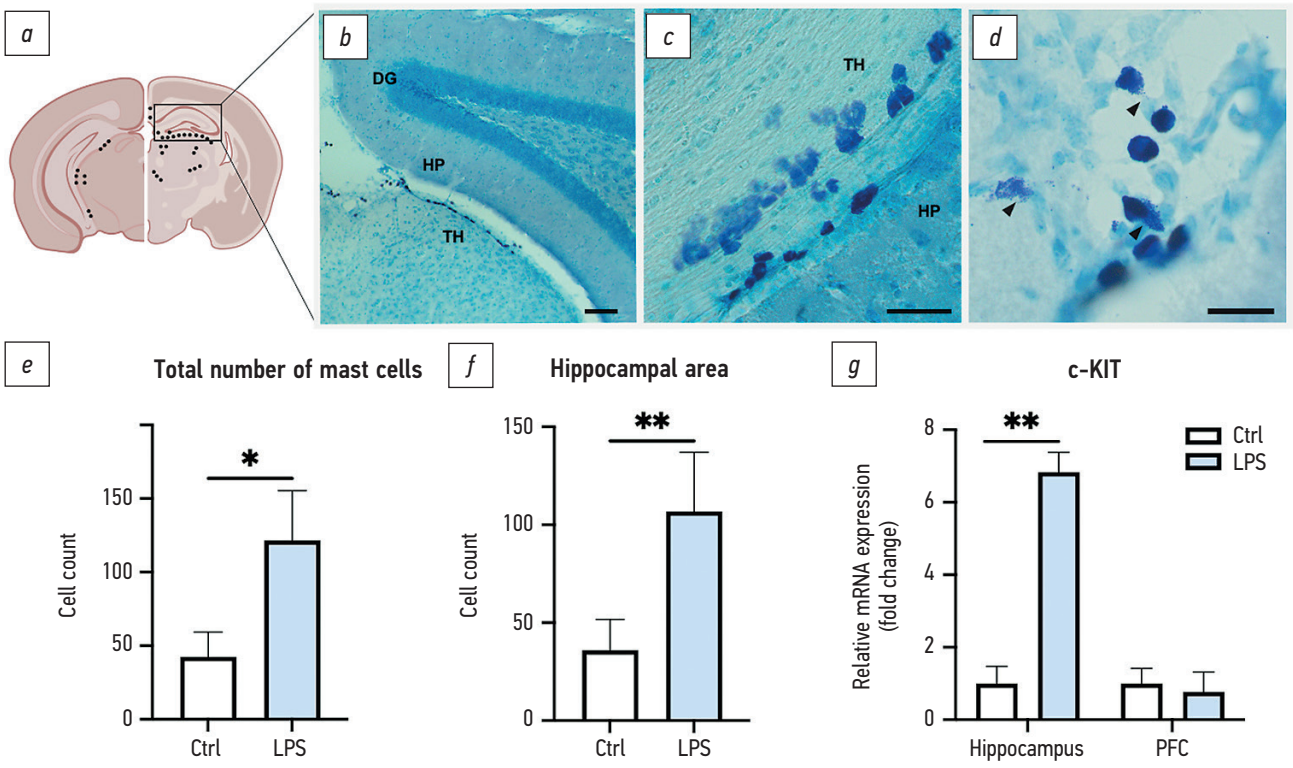

Рис. 5. Тучные клетки в мозге мышей после введения LPS: *a* — распределение тучных клеток на фронтальном срезе мозга мыши; *b–d* — соответствующие микрофотографии, показывающие окрашенные гранулоциты в периваскулярном пространстве между гиппокампом и таламусом; *e*, *f* — общее количество тучных клеток, идентифицированных на срезах головного мозга, и отдельно в области гиппокампа, включая периваскулярное пространство между HP и TH; *g* — уровень экспрессии c-KIT в ответ на инъекции LPS. Стрелки на рис. *d* указывают на тучные клетки в процессе дегрануляции. LPS — липополисахарид, Ctrl — контрольная группа, HP — гиппокамп, TH — таламус, DG — зубчатая извилина, PFC — префронтальная кора; *n*=10/8 (Ctrl/LPS) для рис. *e*, *f*; *n*=9/10 (Ctrl/LPS) для рис. *g*. Бар 100 мкм (*b*); 50 мкм (*c*); 25 мкм (*d*). Данные представлены как средние ± SEM; * $p \leqslant 0{,}05$; ** $p \leqslant 0{,}01$ (t-тест, тест Манна–Уитни).

Fig. 5. Mast cells in the mice brain after LPS treatment: *a*, distribution of mast cells in the frontal section of the mice brain; *b–d*, corresponding micrographs showing stained granulocytes in the perivascular space between the hippocampus and thalamus; *e*, *f*, total count of mast cells identified in brain slices and the hippocampal area, including the perivascular space between HP and TH; *g*, c-KIT expression in response to LPS injections. Arrowheads in *d* show degranulating mast cells. LPS, lipopolysaccharide; Ctrl, control group; HP, hippocampus; TH, thalamus; DG, dentate gyrus; PFC, prefrontal cortex; *n* = 10/8 (Ctrl/LPS) for *e*, *f*; *n* = 9/10 (Ctrl/LPS) for *g*. Scale bar = 100 (*b*), 50 (*c*), and 25 (*d*) μm. Data are presented as mean values ± SEM; * $p \leqslant 0.05$, ** $p \leqslant 0.01$ (*t*-test, MannWhitney test).

Lipopolysaccharide Induced M1 Microglia Phenotype *In Vitro* Resolved by FGF2

In addition to *in vivo* analysis of microglia, we also employed a primary culture glial cell model to verify that the observed effects of LPS and FGF2 result from the direct effect on microglial cells rather than being mediated by systemic immune or neurovascular mechanisms. This approach allowed for a more isolated examination of the effects of LPS on microglial morphology and assessment of whether FGF2 could prevent or reverse the activation of these cells.

Analysis of microglial phenotype ratios revealed that in the presence of FGF2 and in the control group, microglia predominantly had a ramified phenotype, indicating a non-activated state (Fig. 8, a, c). In contrast, when cultured with LPS, most cells in the microglial population shifted towards the amoeboid phenotype, suggesting their pro-inflammatory activation. Under the influence of FGF2 in neuroinflammation conditions, a redistribution of cell phenotypes was observed, including ramified and amoeboid microglia. Morphological assessment of Iba1+ cells (see Fig. 8b) showed that the largest area of microglial cells, as compared to the control group, was observed under conditions of induced neuroinflammation. The smallest area was detected at 12 hours of FGF2 exposure. The graph shows significant differences in microglial area between the control groups and those co-cultured with FGF2 and LPS at 6 and 12 hours. Comparative analysis revealed statistically significant differences in microglial area between experimental groups cultured with LPS and co-cultured with LPS and FGF2. This indicates that FGF2 reduced the microglial cell area under induced neuroinflammation conditions by 10.8% and 13.9% at 6 and 12 hours, respectively.

Thus, the morphological shift towards the amoeboid phenotype in response to LPS was successfully reproduced *in vitro*, confirming that microglia directly respond to the inflammatory stimulus. FGF2 added to the culture medium reduced the microglial cell body area and promoted the

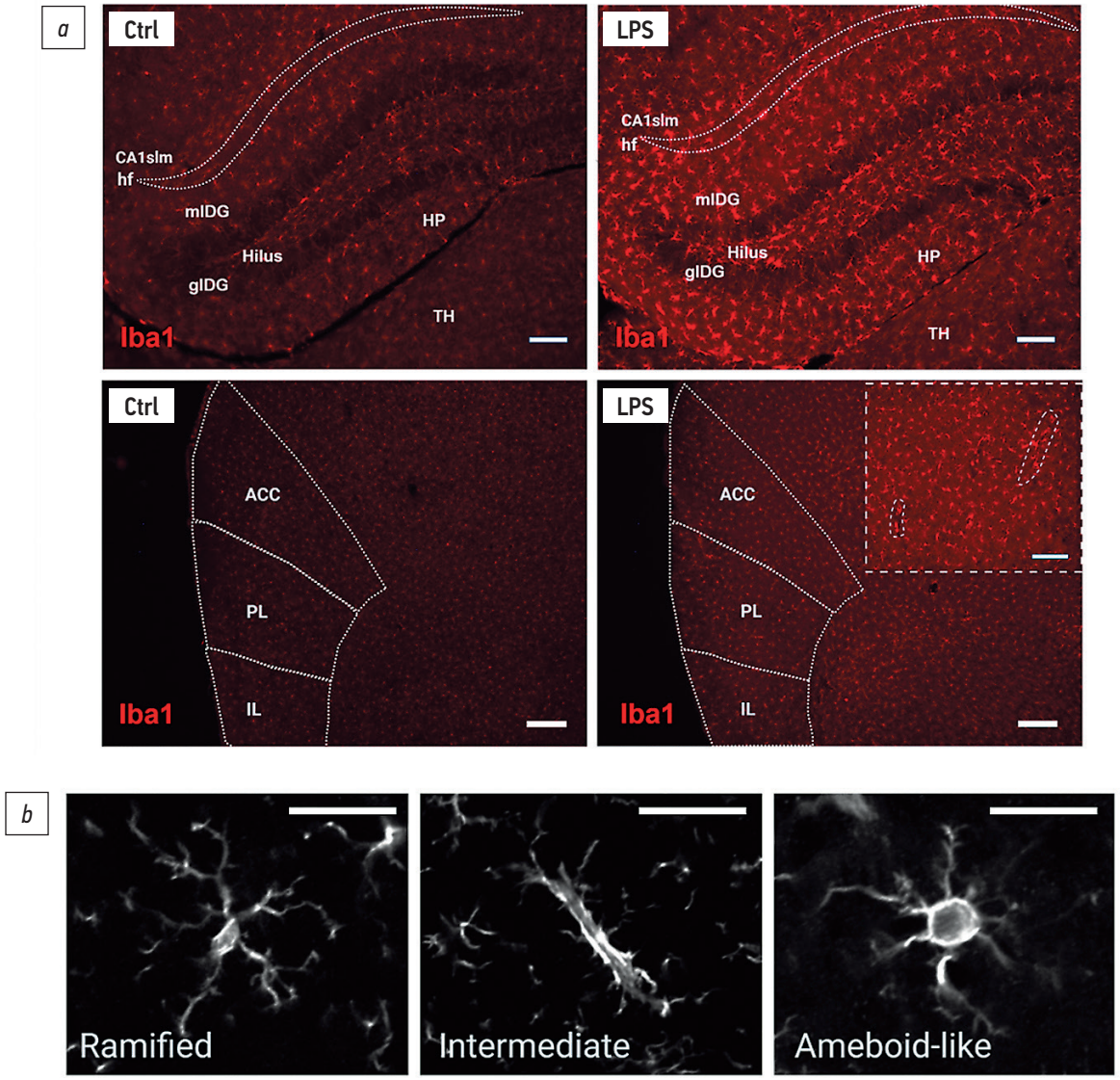

Рис. 6. Пролиферация микроглии в ответ на LPS в mlDG, glDG, хилус гиппокампа, периваскулярной области между HP и TH, периваскулярной области между DG и CA1slm, областях mPFC (ACC, PL, IL) и периваскулярных пространствах mPFC: *a* — репрезентативные иммуногистохимические изображения Iba1 (красная флуоресценция) в гиппокампе и области mPFC, полученные с помощью флуоресцентной микроскопии; *b* — репрезентативные изображения с конфокального микроскопа разветвлённого, промежуточного и амебоидного фенотипов Iba1+ клеток; *c*, *d* — процентное соотношение фенотипов микроглии и площади клеток микроглии в гиппокампе и области mPFC; *e* — уровень экспрессии Iba1 в гиппокампе и префронтальной коре мышей в ответ на хроническое введение LPS; *f–h*, *j* — количество Iba1+ клеток, *i* — CTCF Iba1+ клеток в периваскулярной области между DG и CA1slm. LPS — липополисахарид, Ctrl — контрольная группа, Iba1 — ионизированная кальций-связывающая адапторная молекула 1, HP — гиппокамп, TH — таламус, DG — зубчатая извилина, mlDG — молекулярный слой зубчатой извилины, glDG — гранулярный слой зубчатой извилины, hilus — хилус, CA1slm — stratum lacunosum-moleculare поля CA1, hf — гиппокампальная щель, mPFC — медиальная префронтальная кора, ACC — передняя поясная кора, PL — прелимбическая кора, IL — инфралимбическая кора; *n*=9/10 (Ctrl/LPS) для рис. *e*, *n*=10/9 (Ctrl/LPS) для рис. c, *d*, *f–j*. Бар 100 мкм для области гиппокампа, 200 мкм для mPFC, 20 мкм для фенотипов Iba1+ клеток. Данные представлены как средние ± SEM; * $p \leqslant 0{,}05$; ** $p \leqslant 0{,}01$; **** $p \leqslant 0{,}0001$ (t-тест, тест Манна–Уитни).

Fig. 6. Microglial proliferation in response to LPS administration in the mlDG, glDG, hippocampal hilus, perivascular area between HP and TH, perivascular area between DG and CA1slm, mPFC regions (ACC, PL, and IL), and perivascular area vessels of mPFC: *a*, representative fluorescent microscopy immunohistochemical images of Iba1 (red fluorescence) in the hippocampus and mPFC area; *b*, representative confocal microscopy immunohistochemical images of the ramified, intermediate and ameboid phenotypes of Iba1+ cells; *c*, *d*, percentage ratio of microglial phenotypes and microglial area in the hippocampus and mPFC area; *e*, expression of Iba1 in the hippocampus and prefrontal cortex of mice in response to chronic LPS treatment; *f–h*, *j* Iba1+ cell count; *i*, CTCF of Iba1+ cells in the perivascular area between DG and CA1slm. LPS, lipopolysaccharide; Ctrl, control group; Iba1, ionized calcium-binding adaptor molecule 1; HP, hippocampus; TH, thalamus; DG, dentate gyrus; mlDG, molecular layer of dentate gyrus; glDG, granular layer of dentate gyrus; CA1slm, stratum lacunosum-moleculare of CA1 field; hf, hippocampal fissure; mPFC, medial prefrontal cortex; ACC, anterior cingulate cortex; PL, prelimbic cortex; IL, infralimbic cortex; *n* = 9/10 (Ctrl/LPS) for *e*; *n* = 10/9 (Ctrl/LPS) for *c*, *d*, *f–j*. Scale bar = 100 μm for the hippocampal area, 200 μm for mPFC, 20 μm for Iba1+ phenotypes. Data are presented as mean values ± SEM; * $p \leqslant 0.05$, ** $p \leqslant 0.01$, **** $p \leqslant 0.0001$ (*t*-test, Mann–Whitney test).

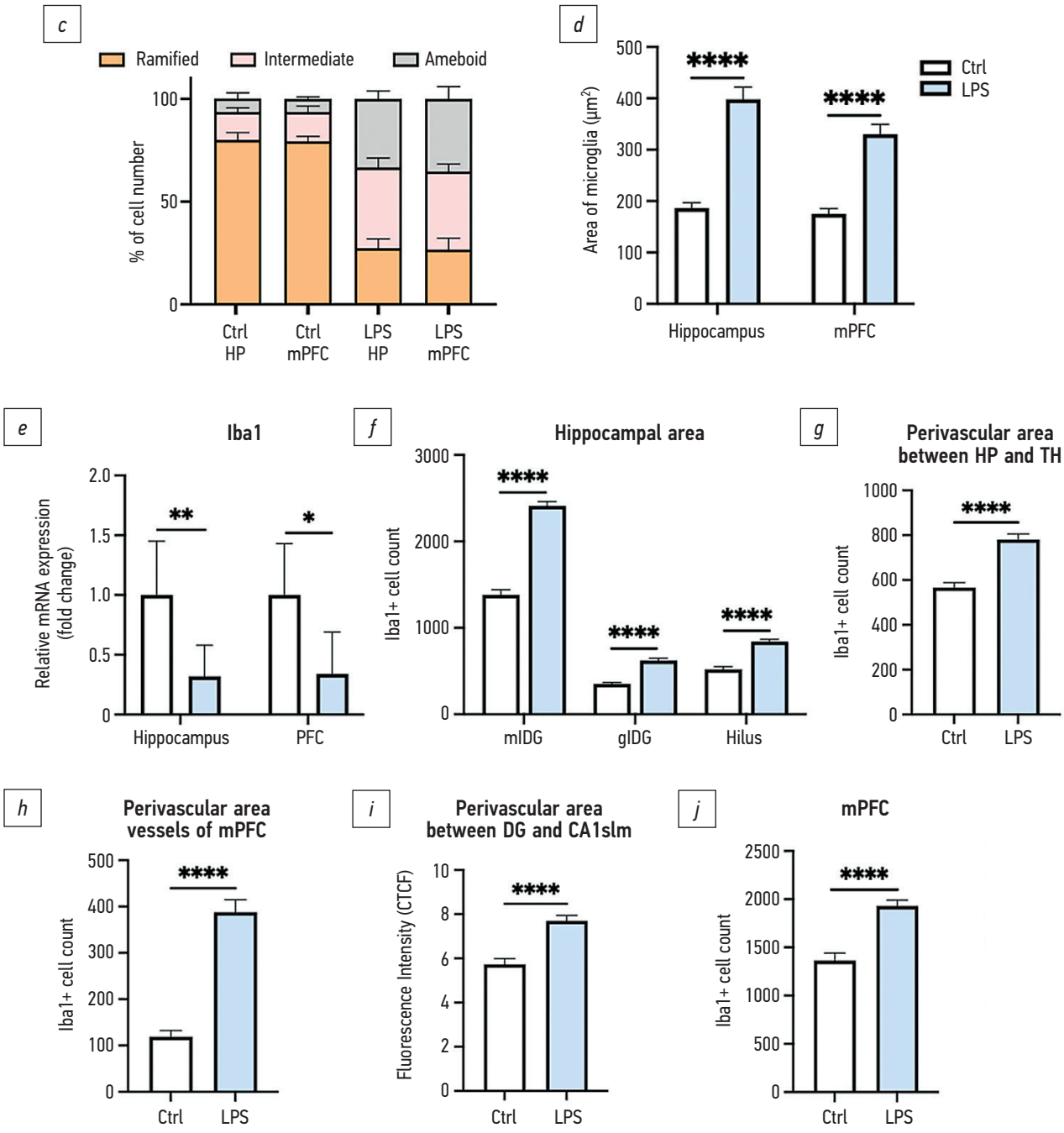

Рис. 6. Окончание.
Fig. 6. The End.

restoration of the proportion of ramified cells, indicating the anti-inflammatory effect of FGF2 at the cellular level. These *in vitro* findings corroborate the *in vivo* data, where lower FGF2 expression was associated with enhanced microglial activation in the hippocampus and the PFC. Thus, the use of the cell culture model was critical for the functional validation of the FGF2 role as a potential neuroprotective agent and inflammation modulator in the central nervous system. We suggest that *in vitro* findings support the hypothesis of cell-autonomous mechanisms of FGF2 action and highlight its therapeutic potential as a target in inflammation-associated depression.

Lipopolysaccharide Affects the Expression of Glutamate Receptors, Transporters, and Glutamate Metabolism-Related Genes in the Brain

We examined the effect of LPS on the expression of ionotropic glutamatergic receptor subunits NR2A and GluR1; metabotropic receptors mGluR1 and mGluR3; glutamate transporters, including vesicular glutamate transporter 1 (VGLUT1), glial high affinity glutamate transporter (GLAST), glutamate transporter 1 (GLT-1), glutamate/gamma-aminobutyric acid (GABA) metabolism-related enzymes,

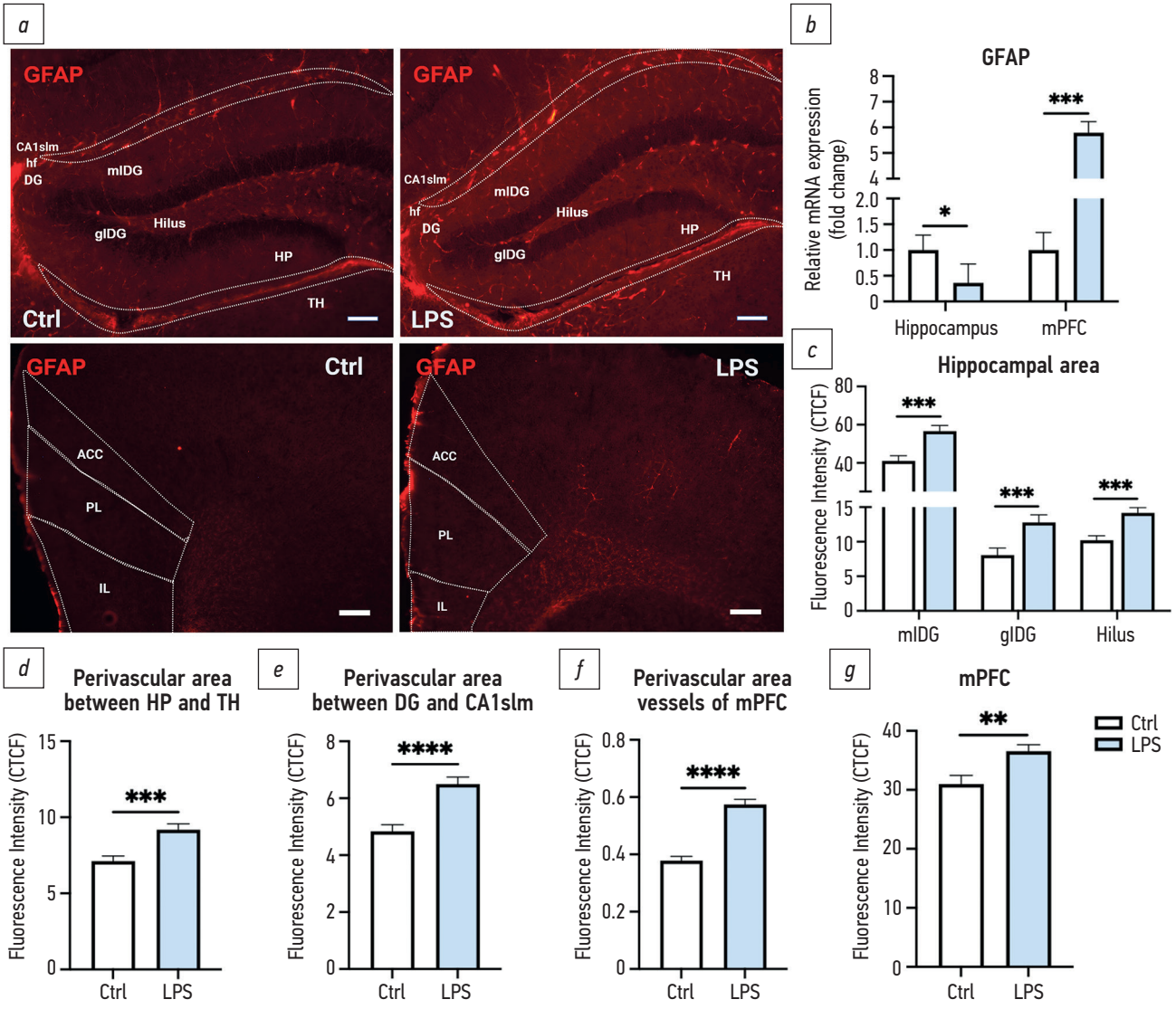

Рис. 7. Интенсивность флуоресценции GFAP+ клеток в ответ на LPS в mlDG, glDG, хилусе гиппокампа, периваскулярной области между HP и TH, периваскулярной области между DG и CA1slm, областях mPFC (ACC, PL, IL) и периваскулярных пространствах mPFC: *a* — репрезентативные флуоресцентно-микроскопические иммуногистохимические изображения GFAP (красная флуоресценция) в области гиппокампа и mPFC; *b* — уровень экспрессии GFAP в гиппокампе и префронтальной коре мышей в ответ на хроническое введение LPS; *c–e* — CTCF GFAP+ клеток в области гиппокампа, периваскулярной области между HP и TH, периваскулярной области между DG и CA1slm; *f*, *g* — CTCF GFAP+ клеток в mPFC и периваскулярных пространствах mPFC. LPS — липополисахарид, Ctrl — контрольная группа, GFAP — глиальный фибриллярный кислый белок, HP — гиппокамп, TH — таламус, DG — зубчатая извилина, mlDG — молекулярный слой зубчатой извилины, glDG — гранулярный слой зубчатой извилины, CA1slm — stratum lacunosum-moleculare поля CA1, hf — гиппокампальная щель, mPFC — медиальная префронтальная кора, ACC — передняя поясная кора, PL — прелимбическая кора, IL — инфралимбическая кора, *n*=9/10 (Ctrl/LPS) для рис. *b*, *n*=10/9 (Ctrl/LPS) для рис. *c–g*. Бар 100 мкм для области гиппокампа, 200 мкм для mPFC. Данные представлены как средние ± SEM; * $p \leqslant 0{,}05$; ** $p \leqslant 0{,}01$; *** $p \leqslant 0{,}001$; **** $p \leqslant 0{,}0001$ (t-тест, тест Манна–Уитни).

Fig. 7. Fluorescence intensity of GFAP+ cells in response to LPS administration in the mlDG, glDG, hippocampal hilus, perivascular area between HP and TH, perivascular area between DG and CA1slm, mPFC regions (ACC, PL, and IL), and perivascular area vessels of mPFC: *a*, representative fluorescent microscopy immunohistochemical images of GFAP (red fluorescence) in the hippocampus and mPFC area; *b*, expression of GFAP in the hippocampus and PFC of mice in response to chronic LPS treatment; *c–e*, CTCF of GFAP+ cells in the hippocampal area, perivascular area between HP and TH, perivascular area between DG and CA1slm; *f*, *g*, CTCF of GFAP+ cells in the mPFC and perivascular area vessels of mPFC. LPS, lipopolysaccharide; Ctrl, control group; GFAP, glial fibrillary acidic protein; HP, hippocampus; TH, thalamus; DG, dentate gyrus; mlDG, molecular layer of dentate gyrus; glDG, granular layer of dentate gyrus; CA1slm, stratum lacunosum-moleculare of CA1 field; hf, hippocampal fissure; mPFC, medial prefrontal cortex; ACC, anterior cingulate cortex; PL, prelimbic cortex; IL, infralimbic cortex; *n* = 9/10 (Ctrl/LPS) for *b*; *n* = 10/9 (Ctrl/LPS) for *c–g*. Scale bar = 100 μm for the hippocampal area; 200 μm for mPFC. Data are presented as mean values ± SEM; * $p \leqslant 0.05$, ** $p \leqslant 0.01$, *** $p \leqslant 0.001$, **** $p \leqslant 0.0001$ (*t*-test, Mann–Whitney test).

glutamine synthetase (GS), glutaminase (Gls), and glutamate/GABA metabolism-related gene (GAD1) (see Fig. 9, a–i). Gene expression of GluR1, α-amino-3-hydroxy-5-methyl-4-isoxazolepropionic acid receptor (AMPA) subunit 1, was elevated in both brain regions ($p = 0.03$ for the hippocampus; $p = 0.0015$ for the PFC, see Fig. 9b); whereas the expression of NR2A, N-methyl-D-aspartate (NMDA) receptor subunit 2A, was elevated in the hippocampus ($p = 0.0076$) and lower in

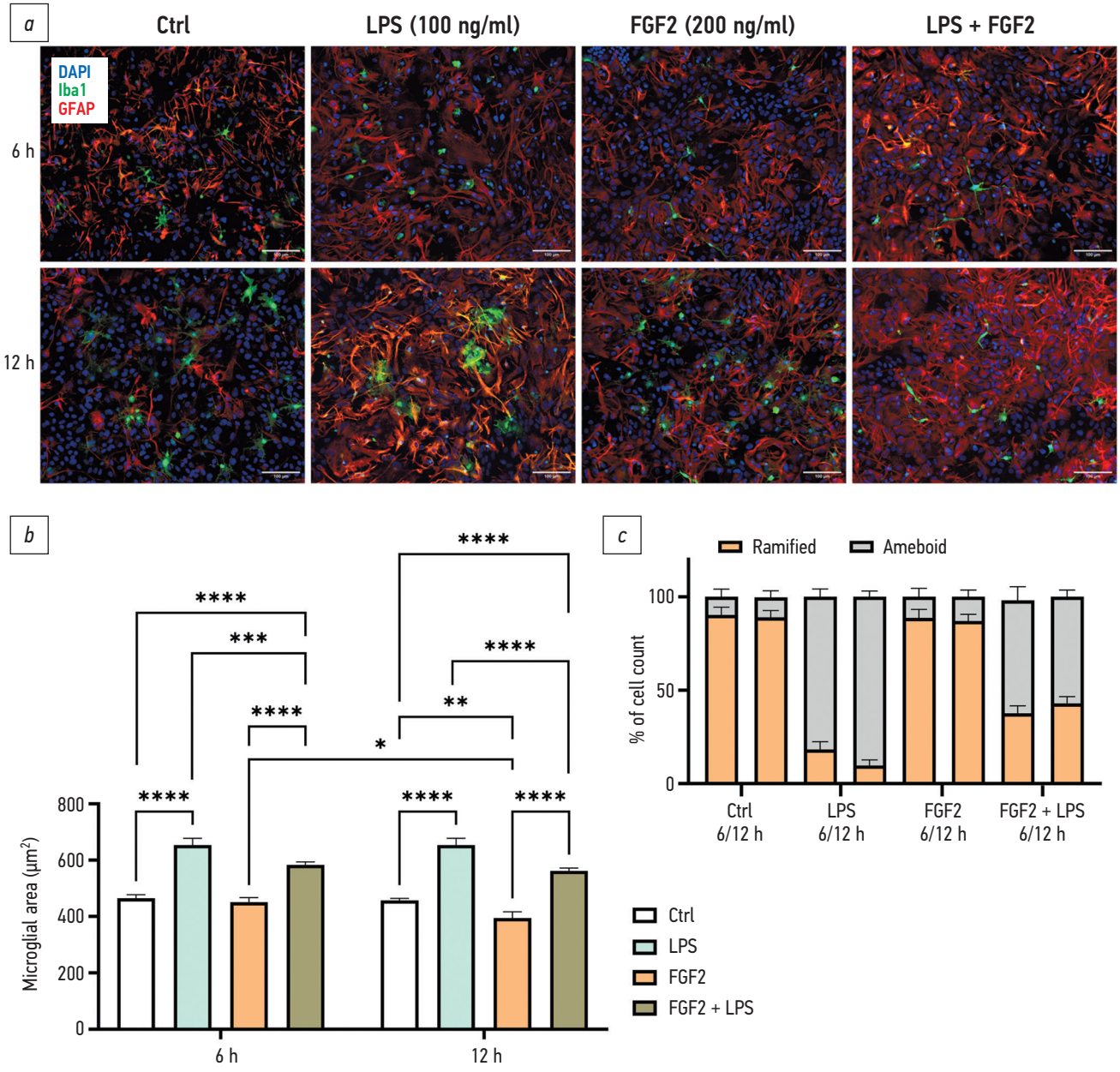

Рис. 8. Процентное соотношение фенотипов микроглии: *a*, *c* — в первичной смешанной глиальной культуре мышей под воздействием LPS и FGF2, *b* — площадь микроглиальных клеток. LPS — липополисахарид, Ctrl — контрольная группа, FGF2 — фактор роста фибробластов 2. Микроглиальные клетки инкубировали с 100 нг/мл LPS и 200 нг/мл FGF2 в течение 6/12 ч. Ramified — разветвленный фенотип, Ameboid — амебоидный фенотип. Бар 100 мкм. Данные представлены как среднее ± SD (*n*=3, независимые эксперименты); * $p \leqslant 0{,}05$; ** $p \leqslant 0{,}01$; *** $p \leqslant 0{,}001$; **** $p \leqslant 0{,}0001$ (двухфакторный тест ANOVA).

Fig. 8. Percentage ratio of microglial phenotypes: *a*, *c*, in mixed glial primary culture of mice under the influence of LPS and FGF2; *b*, microglial area. LPS, lipopolysaccharide; Ctrl, control group; FGF2, fibroblast growth factor 2. Microglia were treated with 100 ng/mL LPS and 200 ng/mL FGF2 for 6/12 h. Ramified — phenotype with highly arborized branches, Ameboid — ameboid-like phenotype. Scale bar = 100 μm. Data are presented as mean values ± SD (*n* = 3, independent experiments); * $p \leqslant 0.05$, ** $p \leqslant 0.01$, *** $p \leqslant 0.001$, **** $p \leqslant 0.0001$ (ANOVA).

the PFC ($p < 0.0001$) compared to the control group (see Fig. 9a). LPS administration significantly increased the expression of metabotropic receptors mGluR1 ($p = 0.0001$ for the hippocampus; $p = 0.0045$ for PFC, see Fig. 9c) and mGluR3 ($p = 0.0005$ for the hippocampus; $p = 0.142$ for PFC, see Fig. 9d) genes both in the hippocampus and the PFC. Expression of VGLUT1 gene, a vesicular glutamate transporter, was found to be significantly elevated in the hippocampus ($p = 0.0353$) and decreased in the PFC ($p = 0.0191$, see Fig. 9f). In addition, the expression of another glutamate transporter, GLAST, was elevated in both brain regions ($p < 0.0001$ for the hippocampus; $p = 0.0001$ for PFC, see Fig. 9e). After LPS treatment, the expression of glutamate metabolism-related gene GS was significantly lower in the hippocampus ($p = 0.0382$); whereas its expression in the PFC was elevated ($p = 0.008$, see Fig. 9g). The expression of another glutamate metabolism-related gene, glutaminase (Gls) A was upregulated in the hippocampus ($p = 0.04$);

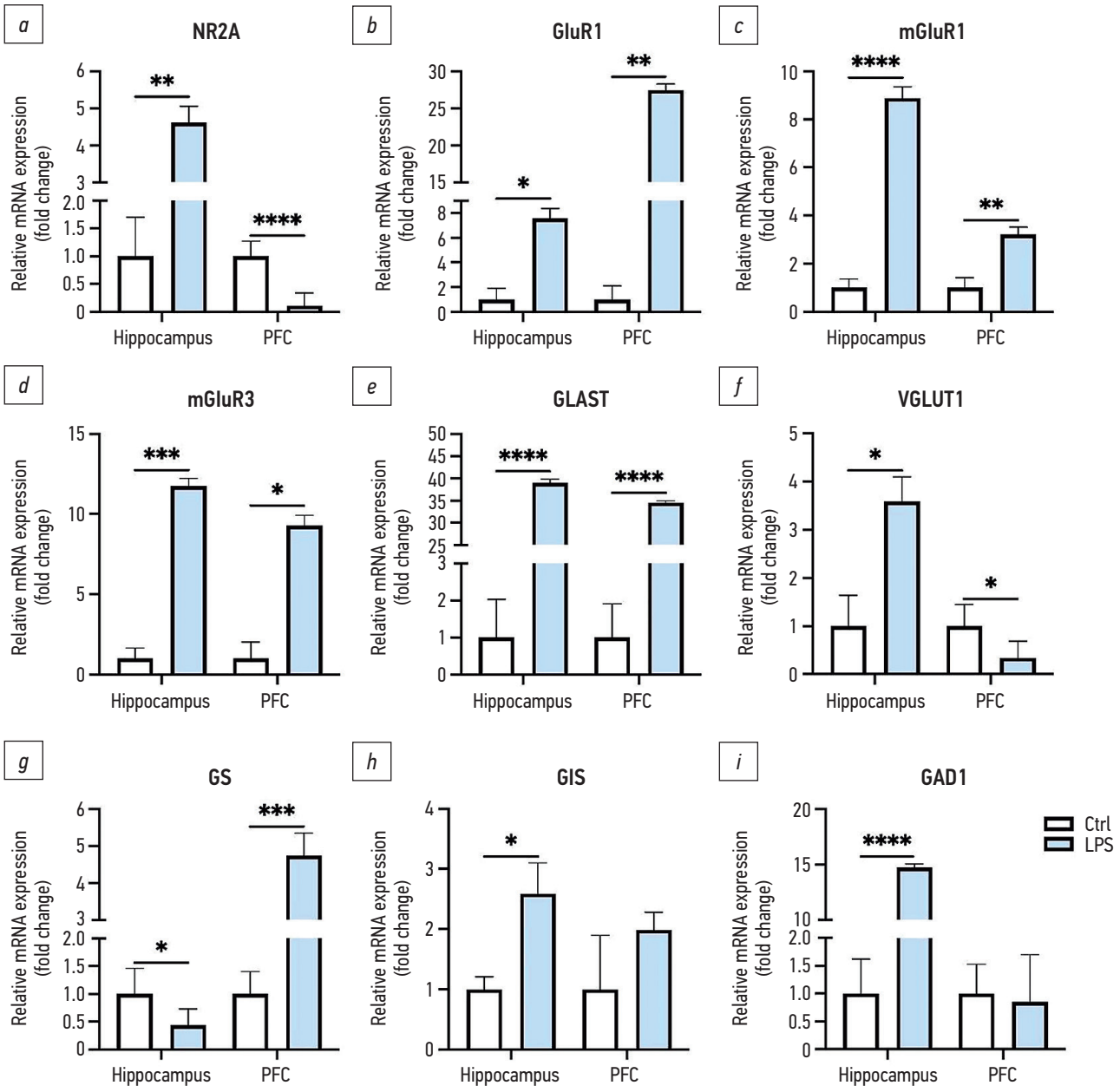

Рис. 9. Уровни экспрессии рецепторов и транспортеров глутамата/ГАМК и генов, связанных с метаболизмом глутамата, в гиппокампе и префронтальной коре мышей в ответ на хроническое введение LPS: *a–i* — уровни экспрессии генов. LPS — липополисахарид, Ctrl — контрольная группа, mRNA — матричная рибонуклеиновая кислота, NR2A — субъединица 2A глутаматного ионотропного рецептора NMDA, GluR1 — субъединица 1 глутаматного ионотропного рецептора AMPA, mGluR1 — глутаматный метаботропный рецептор 1, mGluR3 — глутаматный метаботропный рецептор 3, GLAST — глутаматный/аспартатный транспортер 1, VGLUT1 — везикулярный глутаматный транспортер 1, GS — глутамат синтетаза (глутамат-аммиак лигаза), Gls — глутаминаза, GAD1 — глутамат декарбоксилаза 1, PFC — префронтальная кора; *n*=9/10 (Ctrl/LPS). Данные представлены как средние ± SEM; * $p \leqslant 0{,}05$; ** $p \leqslant 0{,}01$; *** $p \leqslant 0{,}001$; **** $p \leqslant 0{,}0001$ (t-тест, тест Манна–Уитни).

Fig. 9. Expression of Glutamate/GABA receptors and transporters and glutamate metabolism-related genes in the hippocampus and prefrontal cortex of mice in response to chronic LPS treatment: *a–i*, gene expression. LPS, lipopolysaccharide; Ctrl, control group; mRNA, messenger ribonucleic acid; NR2A, glutamate ionotropic receptor NMDA type subunit 2A; GluR1, glutamate ionotropic receptor AMPA type subunit 1; mGluR1, glutamate metabotropic receptor 1; mGluR3, glutamate metabotropic receptor 3; GLAST, glutamate/aspartate transporter 1; VGLUT1, vesicular glutamate transporter 1; GS, glutamine synthetase (glutamate ammonia ligase); Gls, glutaminase; GAD1, glutamate decarboxylase 1; PFC, prefrontal cortex; *n* = 9/10 (Ctrl/LPS). Data are presented as mean values ± SEM; * $p \leqslant 0.05$, ** $p \leqslant 0.01$, *** $p \leqslant 0.001$, **** $p \leqslant 0.0001$ (*t*-test, Mann–Whitney test).

whereas (p = 0.3095) no significant changes were detected in the PFC (see Fig. 9h). Moreover, the expression of GAD1 was elevated in the hippocampus ($p < 0.0001$), but there was no significant changes in the PFC (p = 0.0159) compared to control animals (see Fig. 9i).

In contrast to the elevated expression of GLAST (see Fig. 9e), expression of another glutamate transporter, GLT-1, was significantly lower in the hippocampus (p = 0.0001) and higher in the PFC (p = 0.0014, see Fig. 10d). Next, we investigated the CTCF of GLT-1+ cells in the hippocampal

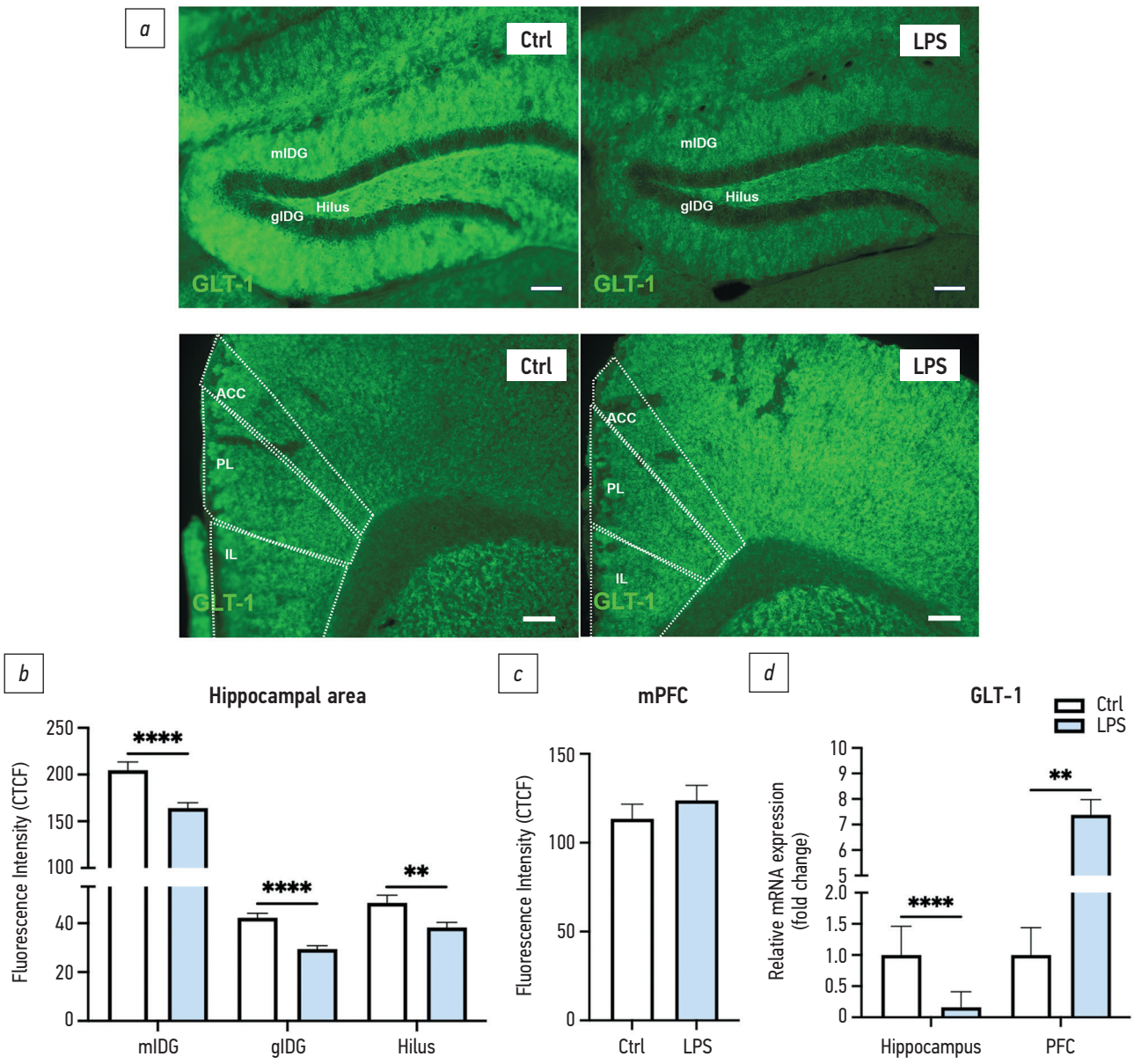

Рис. 10. Интенсивность флуоресценции GLT-1+ клеток в области гиппокампа и mPFC и уровень экспрессии гена GLT-1 в ответ на хроническое введение LPS: *a* — репрезентативные флуоресцентно-микроскопические иммуногистохимические изображения GLT-1 (зелёная флуоресценция) в mlDG, glDG и хилус гиппокампа, а также в областях mPFC (ACC, PL, IL); *b* — CTCF GLT-1+ клеток в области гиппокампа; *c* — CTCF GLT-1+ клеток в mPFC; *d* — относительная экспрессия мРНК GLT-1. CTCF — скорректированная общая флуоресценция клеток, LPS — липополисахарид, Ctrl — контрольная группа, GLT-1 — глутаматный транспортер 1, mlDG — молекулярный слой зубчатой извилины, glDG — гранулярный слой зубчатой извилины, mPFC — медиальная префронтальная кора, ACC — передняя поясная кора, PL — прелимбическая кора, IL — инфралимбическая кора, PFC — префронтальная кора; *n*=10/9 (Ctrl/LPS) для рис. *b–c*, *n*=9/10 (Ctrl/LPS) для рис. *d*. Бар 100 мкм для области гиппокампа, 200 мкм для mPFC. Данные представлены как средние ± SEM; ** $p \leqslant 0{,}01$; **** $p \leqslant 0{,}0001$ (t-тест, тест Манна–Уитни).

Fig. 10. Fluorescence intensity of GLT-1+ cells in the hippocampal area and mPFC and expression of the GLT-1 gene in response to chronic LPS treatment: *a*, representative fluorescent microscopy immunohistochemical images of GLT-1 (green fluorescence) in the mlDG, glDG, hippocampal hilus, and mPFC regions (ACC, PL, and IL); *b*, CTCF of GLT-1+ cells in the hippocampal area; *c*, CTCF of GLT-1+ cells in mPFC; *d*, relative mRNA expression of GLT-1. CTCF, corrected total cell fluorescence; LPS, lipopolysaccharide; Ctrl, control group; GLT-1, glutamate transporter 1; mlDG, molecular layer of dentate gyrus; glDG, granular layer of dentate gyrus; mPFC, medial prefrontal cortex; ACC, anterior cingulate cortex; PL, prelimbic cortex; IL, infralimbic cortex; PFC, prefrontal cortex; *n* = 10/9 (Ctrl/LPS) for *b–c*; *n* = 9/10 (Ctrl/LPS) for *d*. Scale bar = 100 μm for hippocampal area; 200 μm for mPFC. Data are presented as mean values ± SEM; ** $p \leqslant 0.01$, **** $p \leqslant 0.0001$ (*t*-test, Mann–Whitney test).

regions, such as the molecular (mlDG) and granular (glDG) layers of dentate gyrus and hilus, and mPFC regions, including the infralimbic (IL), prelimbic (PL), and anterior cingulate (ACC) cortex, by fluorescent microscopy using an antibody selective for GLT-1 (see Fig. 10, a–c). Fig. 10b shows that the CTCF was significantly lower in the mlDG ($p < 0.0001$), glDG ($p < 0.0001$), and hilus ($p = 0.0069$); real-time PCR demonstrated similar results for the hippocampal GLT-1. The mPFC showed no significant CTCF differences ($p = 0.3826$, see Fig. 10c).

DISCUSSION

Chronic-interval LPS treatment resulted in anxiety and depressive-like behavior, memory impairment, and weight loss in mice. Weight loss in LPS-treated mice is associated with anorexia, lipid hypoanabolism, and lipid hypercatabolism and this effect is mediated by the toll-like receptor 4 (TLR4), the key well-known LPS receptor [14]. Lower sucrose preference measured during the SPT is a sign of reduced interest in hedonic stimulus and dysregulation in reward processing [15]. However, it is worth noting that our data show the approximate sucrose preference of 60% in mice from the control group, which is generally considered quite low. Depressive-like behavior in LPS-treated mice also included increased immobility in the TST (behavioral despair), lower locomotor activity, and pronounced thigmotaxis in the OFT. This behavioral pattern is a well-known effect of endotoxin treatment (inflammation-associated depressive-like state) [3]. In addition, we have found that LPS-treated mice behaved abnormally in the Y-maze test; they showed decreased spontaneous alternation, a measure of spatial working memory (prefrontal cortical functions), and decreased number of novel arm entries, i.e. impaired spatial reference memory (hippocampal functions) [16]. Data on LPS-induced spatial memory impairment are contradictory. Czerniawski et al. showed that injecting LPS at 6 hours before behavior testing impairs retrieval of context-object discrimination, but not spatial memory, i.e. LPS-induced inflammation disrupts pattern separation processing in the hippocampus [17]. However, Zong et al. [18] and Dastan et al. [19] demonstrated that LPS induces spatial memory deficit as tested in Morris water maze test. Thus, we decided to investigate cellular and molecular changes in response to LPS administration in these two brain regions.

LPS injections promoted the expression of TNF-α, IL-1β, IL-6, and IL-10 cytokines in the spleen. Spleen is a first order response organ in case of intraperitoneal LPS injections [20]; thus, these expression changes were expected and indicate ongoing inflammation. TNF-α is an early mediator of inflammation; its main source during the development of a systemic immune response is tissue-resident macrophages. The brain controls the innate immune response by activating the vagus and splenic nerves and subsequent interaction with acetylcholine receptors on macrophages in the spleen, inhibiting the production of pro-inflammatory cytokines, including TNF-α [21]. As our protocol provided for chronic LPS treatment with a recovery period, higher IL-10 levels in the spleen may be interpreted as an early anti-inflammatory action. We did not observe increased IL-10 expression in the brain, indicating ongoing neuroinflammation (elevated expression of TNF-α and IL-1β in the PFC and the hippocampus). Moreover, IL-10 was significantly downregulated in the hippocampus, but not in the PFC. Microglial cells are the key factors of neuroinflammation; however, immune signal transmission from the blood to the brain include the activation of endothelial cells and may modulate tight junction protein expression. PCR assay revealed substantially increased TJP1/ZO1 expression both in the hippocampus and the PFC of LPS-treated mice, indicating that the barrier function of BBB is preserved. This is consistent with previous studies showing that LPS, even when administered repeatedly, does not substantially increase the BBB permeability [7]. TJP1 is critical to the assembly of the other tight junction proteins, such as claudins and occluding [22, 23]; the expression of the latter decreased significantly after LPS treatment in our experiments. Although occludin-deficient [24] and claudin 3-deficient mice [25] do not demonstrate BBB disruption, recent findings indicate that the modified expression of occludin is associated with the regulation of HIV-1 infection in the brain [26], and modulation of BBB integrity and neurological function after ischemic stroke [27]. Thus, we can conclude that BBB barrier function is preserved after chronic-interval LPS treatment, but paracellular signaling may be altered. Consistently with this, we found a significantly increased expression of VEGFA in the hippocampus and the PFC. VEGFA promotes phosphorylation of TJP1 and occluding [28], which is accompanied by their downregulation or reorganization [29]. In addition, VEGFA acts as chemoattractant for macrophages [30] and promotes migration and proliferation of astrocytes [31]. The expression of E-selectin, an endothelial-leukocyte adhesion molecule, also increased substantially in the hippocampus and the PFC of LPS-treated mice. It is well-known that TNF-α [32] and IL-1 [33] promote E-selectin expression by endothelial cells, helping to recruit leukocytes to an injury and/or infection site. At the same time, the expression of FGF2, a basic fibroblast growth factor, decreased in both brain regions after LPS treatment. Low levels of FGF2 are associated with increased anxiety [34] and exogenous FGF2 reverses depressive-like symptoms and restores neuroinflammation-impaired adult neurogenesis in the hippocampus [35]. Moreover, application of FGF2 on endothelial cells compromised by LPS reduces BBB dysfunction [36]; whereas the intraventricular injection of FGF2 reversed the LPS-induced depressive-like behaviors and inhibited hippocampal microglia activation [37].

In line with an elevated VEGFA and E-selectin expression in LPS-treated mice, we have found an increased number of mast cells in their brains and elevated c-KIT (a gene essential for mast cell survival, differentiation, and degranulation) expression in the hippocampus (but not the PFC). The role of mast cells in the central nervous system is still understudied. Mast cells are present near the barrier surfaces and release inflammatory, vasoactive, nociceptive, and neuroprotective mediators [38], such as TNF-α, FGF2, matrix metalloproteinases (MMPs), serine proteases, serotonin, histamine, nerve growth factor (NGF), and angiogenin [39]. MMPs are capable of degrading the components of an extracellular matrix and even compromise the BBB function [40, 41]. Serine proteases have been found to promote TNF-α and TLR4 expression, while reducing

the expression of occludin and claudin 5 [40]. Histamine secreted by mast cells can act as a neuroprotective factor during excitotoxicity by enhancing the activity of glutamate transporters and glutamine synthetase (GS) expression [42]. Mast cells also release serotonin [43], which has been shown to contribute to hippocampal function [44–46]. We have detected multiple mast cells at the degranulation stage in the perivascular space between the hippocampus and thalamus in LPS-treated mice, suggesting they secrete mediators to regulate BBB function and neuroinflammation.

Analysis of astroglial cells revealed the decrease of GFAP expression in the whole hippocampus, while fluorescence intensity of GFAP+ cells in the selected areas (mlDG, glDG, hilus, and perivascular spaces) increased in the LPS group compared to the control groups. This may indicate activation of astroglial cells in these areas of the hippocampus and overall regional heterogeneity of astrocytes in response to LPS. Perez-Dominguez et al. have demonstrated that repeated LPS exposure (4 injections, 1 injection/week at 1 mg/kg) does not elicit reactive changes in astrocytes and elevation of GFAP expression in the hippocampus [47]. In the PFC, the expression of GFAP increased; thus, increased fluorescence intensity of GFAP+ cells in the medial PFC indicates ongoing inflammation. Therefore, LPS injections differently affect the hippocampal and cortical GFAP+ astrocytes. Remarkably, LPS substantially decreased the expression of the microglial marker Iba1. As we used chronic-interval LPS treatment, this may indicate unknown aspects of microglial phenotype changes in response to inflammatory stimuli. Although the expression of Iba1 decreased in the whole hippocampus and the PFC, the number of Iba1+ cells in the analyzed regions (mlDG, glDG, hilus, and mPFC) increased significantly. An increased count of Iba1+ cells may be promoted by proliferation, migration of microglia or peripheral Iba1+ macrophages, or expression of Iba1 by the cells that were poorly visible before LPS stimulation (if these cells had low Iba1 expression in control animals and were not detected). In addition, microglial cell area significantly increased in LPS-treated mice, indicating the microglial activation in response to inflammation. This increase reflects the transition of microglia from a ramified resting state to an amoeboid activated state characteristic of an inflammatory response. Thus, downregulation of Iba1 expression did not affect ameboid microglial phenotype. It is believed that microglia is the main source of proinflammatory cytokines during neuroinflammation. Thus, we analyzed both *in vivo* microglial morphology using brain slices after intraperitoneal LPS injections and *in vitro* microglial morphology using the hippocampal cell culture after application of LPS. Microglial morphology analysis conducted on brain slices detected significant increase of cell area in LPS-treated mice, i.e. a shift to the ameboid phenotype in response to endotoxin both in the hippocampus and the PFC. Cultured hippocampal microglia responded to LPS as expected and the microglial population shifted towards the amoeboid phenotype, indicating the pro-inflammatory activation of the cells (M1). Application of FGF2 promoted M0/M2 ramified phenotype; thus, FGF2 had an anti-inflammatory effect on microglia. Recent studies have shown that intraventricular injections of FGF2 reverse the inflammation-induced depressive behavior and inhibit microglial activation in the hippocampus [37], suggesting FGF2 as a potential therapeutic target in neuroinflammation studies. However, this assumption requires further research. This is consistent with our data on lower FGF2 expression in the hippocampus after chronic-interval LPS treatment.

Neuroinflammation has a drastic effect on neuronal function. Chronic inflammation is associated with many neurodegenerative disorders, including Alzheimer [48] and Parkinson diseases [49], and severe stress and adaptation disorders, such as the posttraumatic stress disorder [50]. Recent findings have shown that acute neuroinflammation induced by LPS injections leads to neuronal hyperexcitability in the dentate gyrus [51]. Therefore, we investigated the expression of some glutamate receptors, transporters, and genes related to glutamate metabolism in the hippocampus and the PFC of LPS-treated mice. In the hippocampus, we found a significant upregulation of all studied genes except for GS, an enzyme catalyzing conversion of glutamate to glutamine, and the glutamate transporter GLT1 (downregulation of GLT1 was also confirmed by immunohistochemistry assays). Astrocyte-specific GS rapidly converts glutamate to glutamine, which is critical in preventing neuronal excitotoxicity [52], and GLT1 is one of the main astrocytic glutamate transporters. It has been shown that GS downregulation increases the number of degenerating cortical neurons *in vitro* [53] and TNF-α is known to inhibit GLT1 expression [54]. As our study detected GS downregulation in the hippocampus and uoregulation of Gls, glutamate receptors, and VGLUT, we can conclude that glutamate transmission in the hippocampus of LPS-treated mice is enhanced, but astrocytic glutamate clearance may be affected (by increasing the risk of excitotoxicity). Upregulation of GLAST, an astrocytic glutamate transporter, and GAD1 (glutamate decarboxylase) indicate an active glutamate buffering by astrocytes and glutamate to GABA conversion by GABA-ergic neurons in the hippocampus. Thus, other compensatory mechanisms are exploited to avoid excitotoxicity. However, GS expression in the PFC significantly increased after LPS injections (and the expression of GLT1 and all glutamate receptors except for NR2A and VGLUT1). Therefore, LPS-induced neuroinflammation in the PFC also led to enhanced glutamate signaling. However, unlike the hippocampus, GS and GLT1 were found to be upregulated in the PFC, indicating active conversion of glutamate to glutamine and active glutamate buffering, i.e. compensation for excitotoxicity. It may be suggested that the hippocampus is more susceptible to LPS-induced inflammation than the PFC and LPS administration impairs astroglial buffering function more in the hippocampus than the PFC. In general, despite the fact that they are considerably similar in both studied brain regions, LPS-induced brain changesare more pronounced in

the hippocampus, i.e. significant downregulation of IL-6 and IL-10 suggests that the hippocampus may be more prone to long-term neuroinflammation and its effects (compromised astrocytic glutamate buffering).

CONCLUSION

We have studied LPS-induced cellular and molecular changes in two brain regions (PFC and the hippocampus) implicated in depression and spatial working and reference memory in mice. Chronic-interval LPS injections induced depression-like symptoms and weight loss in mice and memory deficits as shown by the Y-maze test. LPS promoted the expression of proinflammatory cytokines TNF-α and IL-1β in the spleen and the brain with significant downregulation of IL-6 and IL-10 in the hippocampus, indicating that the hippocampus may be more prone to long-term neuroinflammation than the PFC. LPS treatment upregulated the expression of TJP1/ZO1 and downregulated the expression of claudin 3 and occludin both in the hippocampus and the PFC, suggesting that BBB function is preserved, but paracellular signaling may be altered. This is further confirmed by the elevated expression of VEGFA, E-selectin,increased count of mast cells in the brain of LPS-treated mice, and increased number of microglia and microglial area in the hippocampus and the PFC. The expression of FGF2 was found to be downregulated in both brain regions in LPS-treated mice, which is consistent with previous studies, indicating its role in depressive behavior in rodents. Cultured hippocampal microglia reacted to LPS with ameboid phenotype (M1), which was resolved by FGF2 application. Thus, exogenous FGF2 probably can resolve LPS-induced neuroinflammation *in vivo* and ameliorate depressive symptoms. However, this assumption needs further investigation. LPS treatment resulted in GS and GLT1 downregulation in the hippocampus, but not in the PFC, indicating the compromised glutamate buffering by the hippocampal and not cortical astrocytes. Our data generally indicate that different brain regions differently respond to LPS treatment and it may contribute to depressive symptoms and memory deficits in mice.

ДОПОЛНИТЕЛЬНАЯ ИНФОРМАЦИЯ

Вклад авторов. А. Исмаилова и К.В. Ичеткина — эксперименты, связанные с введением LPS, поведенческим фенотипированием; полимеразной цепной реакцией и гистологией/иммуногистохимией срезов мозга; М.Р. Шульц и А.С. Шульц — *in vitro* эксперименты и все последующие анализы; Е.А. Курилова — контроль за проведением поведенческого фенотипирования и полимеразной цепной реакции; О.П. Тучина — разработка концепции исследования, администрирование проекта, привлечение финансирования, рецензирование и редактирование текста. Все авторы одобрили рукопись (версию для публикации), а также согласились нести ответственность за все аспекты работы, гарантируя надлежащее рассмотрение и решение вопросов, связанных с точностью и добросовестностью любой её части.

Благодарности. Авторы благодарят рецензентов за важные замечания, которые позволили значительно улучшить статью.

Этическая экспертиза. Все эксперименты, включая количество животных, использованных в исследовании, были одобрены Независимым этическим комитетом Центра клинических исследований Балтийского федерального университета имени Иммануила Канта (протокол № 27/2024 от 1.02.2024).

Согласие на публикацию. Неприменимо.

Источники финансирования. Исследование выполнено при поддержке Федеральной академической программы лидерства «Приоритет 2030» в Балтийском федеральном университете имени Иммануила Канта (номер проекта 123110800174-4).

Раскрытие интересов. Авторы заявляют об отсутствии отношений, деятельности и интересов за последние три года, связанных с третьими лицами (коммерческими и некоммерческими), интересы которых могут быть затронуты содержанием статьи.

Оригинальность. При создании настоящей работы авторы не использовали ранее опубликованные сведения (текст, иллюстрации, данные).

Доступ к данным. Все данные, полученные в настоящем исследовании, доступны в статье и в приложении к ней.

Приложение 1. Распределение животных по группам, количество используемых особей и причины исключений в отдельных экспериментах. DOI: 10.17816/gc655664-4373344

Приложение 2. Последовательности праймеров, используемые для анализа методом количественной полимеразной цепной реакции. DOI: 10.17816/gc655664-4373345

Приложение 3. Оптимизация праймеров в целях достижения высокой специфичности и эффективности амплификации целевой ДНК. DOI: 10.17816/gc655664-4373347

Приложение 4. Электрофореграммы продуктов ПЦР-РВ в агарозном геле после температурного градиента. DOI: 10.17816/gc655664-4373349

Приложение 5. Влияние введения LPS на поведение мышей. DOI: 10.17816/gc655664-4373351

Генеративный искусственный интеллект. При создании настоящей статьи технологии генеративного искусственного интеллекта не использовали.

Рассмотрение и рецензирование. Настоящая работа подана в журнал в инициативном порядке и рассмотрена по обычной процедуре. В рецензировании участвовали три внешних рецензента, один член редакционной коллегии и научный редактор издания.

ADDITIONAL INFORMATION

Author contributions: A.U. Ismailova and K.V. Ichetkina: investigation; M.R. Shults and A.S. Shults: investigation, formal analysis; E.A. Kurilova: supervision; O.P. Tuchina: conceptualization, project administration, funding acquisition, writingreviewing & editing All authors approved the version of the manuscript to be published and agree to be accountable for all aspects of the work, ensuring that questions related to the accuracy or integrity of any part of the work are appropriately investigated and resolved.

Acknowledgements: The authors would like to thank the reviewers for their valuable comments, which allowed to significantly improve the article.

Ethics approval: All experiments, including the number of animals used in the study, were approved by the Independent Ethical Committee of the Clinical Research Center at IKBFU, Kaliningrad, protocol No. 27/2024 dated February 1, 2024.
Consent for publication: Not applicable.
Funding sources: This research was funded by the Russian Federal Academic Leadership Program Priority 2030 at the Immanuel Kant Baltic Federal University (project No.: 123110800174-4).
Disclosure of interests: The authors have no relationships, activities, or interests for the last three years related to for-profit or not-for-profit third parties whose interests may be affected by the content of the article. Statement of originality. No previously published material (text, images, or data) was used in this work.
Data availability statement: All data generated during this study are available in the article and its supplementary material.

Supplement 1: Animal distribution, sample sizes, and exclusions by experiment. DOI: 10.17816/gc655664-4373344

Supplement 2: Primer sequences used for quantitative polymerase chain reaction assay. DOI: 10.17816/gc655664-4373345

Supplement 3: Optimization of primers to achieve high specificity and efficiency of target DNA amplification. DOI: 10.17816/gc655664-4373347

Supplement 4: Electropherograms of RT-PCR products in agarose gel after temperature gradient. DOI: 10.17816/gc655664-4373349

Supplement 5: Effect of LPS treatment on mice behavior. DOI: 10.17816/gc655664-4373351

Generative AI: No generative artificial intelligence technologies were used to prepare this article.
Provenance and peer review: This paper was submitted unsolicited and reviewed following the standard procedure. The review process involved three external reviewers, one member of the editorial board, and the in-house scientific editor.

СПИСОК ЛИТЕРАТУРЫ | REFERENCES

1. Zabrodskii PF. Variation in antiinfectious nonspecific resistance of the organism caused by cholinergic stimulation. *Bull Exp Biol Med*. 1995;120:809–811. doi: 10.1007/BF02445960 EDN: XWTLXW
2. Tracey KJ. The inflammatory reflex. *Nature*. 2002;420(6917):853–859. doi: 10.1038/nature01321
3. Yin R, Zhang K, Li Y, et al. Lipopolysaccharide-induced depression-like model in mice: meta-analysis and systematic evaluation. *Front Immunol*. 2023;14:1181973. doi: 10.3389/fimmu.2023.1181973 EDN: ZDYPQS
4. Wu Y, Fan L, Xia F, et al. Global, regional, and national time trends in incidence for depressive disorders, from 1990 to 2019: an age-period-cohort analysis for the GBD 2019. *Ann Gen Psychiatry*. 2024;23(1):28. doi: 10.1186/s12991-024-00513-1 EDN: CKXBHV
5. Hassamal S. Chronic stress, neuroinflammation, and depression: an overview of pathophysiological mechanisms and emerging anti-inflammatories. *Front Psychiatry*. 2023;14:1130989. doi: 10.3389/fpsyt.2023.1130989 EDN: AKXLCS
6. Mahajan GJ, Vallender EJ, Garrett MR, et al. Altered neuro-inflammatory gene expression in hippocampus in major depressive disorder. *Prog Neuropsychopharmacol Biol Psychiatry*. 2018;82:177–186. doi: 10.1016/j.pnpbp.2017.11.017
7. Banks WA, Robinson SM. Minimal penetration of lipopolysaccharide across the murine blood-brain barrier. *Brain Behav Immun*. 2010;24(1):102–109. doi: 10.1016/j.bbi.2009.09.001
8. Maier SF. Bi-directional immune-brain communication: Implications for understanding stress, pain, and cognition. *Brain Behav Immun*. 2003;17(2):69–85. doi: 10.1016/s0889-1591(03)00032-1 EDN: XORLLD
9. Helm K, Viol K, Weiger TM, et al. Neuronal connectivity in major depressive disorder: a systematic review. *Neuropsychiatr Dis Treat*. 2018;14:2715–2737. doi: 10.2147/NDT.S170989 EDN: WWJFRR
10. Duman RS, Sanacora G, Krystal JH. Altered connectivity in depression: GABA and glutamate neurotransmitter deficits and reversal by novel treatments. *Neuron*. 2019;102(1):75–90. doi: 10.1016/j.neuron.2019.03.013 EDN: EGQQKZ
11. Hu J, Wang P, Wang Z, et al. Fibroblast-conditioned media enhance the yield of microglia isolated from mixed glial cultures. *Cell Mol Neurobiol*. 2023;43(1):395–408. doi: 10.1007/s10571-022-01193-9 EDN: PPJXVZ
12. Schildge S, Bohrer C, Beck K, Schachtrup C. Isolation and culture of mouse cortical astrocytes. *J Vis Exp*. 2013;(71):50079. doi: 10.3791/50079
13. Mecha M, Iñigo PM, Mestre L, et al. An easy and fast way to obtain a high number of glial cells from rat cerebral tissue: A beginners approach. V. 1. *Protocols exchange*. 2011. doi: 10.1038/protex.2011.218
14. Yang Y, Zhong W, Zhang Y, et al. Sustained inflammation induced by LPS leads to tolerable anorexia and fat loss via in mice. *J Inflamm Res*. 2022;15:5635–5648. doi: 10.2147/JIR.S358518 EDN: IHRADL
15. Heshmati M, Russo SJ. Anhedonia and the brain reward circuitry in depression. *Curr Behav Neurosci Rep*. 2015;2(3):146–153. doi: 10.1007/s40473-015-0044-3 EDN: BPLEYN
16. Kraeuter AK, Guest PC, Sarnyai Z. The Y-maze for assessment of spatial working and reference memory in mice. *Methods Mol Biol*. 2019;1916:105–111. doi: 10.1007/978-1-4939-8994-2_10
17. Czerniawski J, Miyashita T, Lewandowski G, Guzowski JF. Systemic lipopolysaccharide administration impairs retrieval of context-object discrimination, but not spatial, memory: Evidence for selective disruption of specific hippocampus-dependent memory functions during acute neuroinflammation. *Brain Behav Immun*. 2015;44:159–166. doi: 10.1016/j.bbi.2014.09.014
18. Zong T, Li N, Han F, et al. Microglial depletion rescues spatial memory impairment caused by LPS administration in adult mice. *PeerJ*. 2024;12:e18552. doi: 10.7717/peerj.18552 EDN: ULHLRJ
19. Dastan M, Rajaei Z, Sharifi M, Salehi H. Gallic acid ameliorates LPS-induced memory decline by modulating NF-κB, TNF-α, and Caspase 3 gene expression and attenuating oxidative stress and neuronal loss in the rat hippocampus. *Metab Brain Dis*. 2024;40(1):12. doi: 10.1007/s11011-024-01441-5 EDN: XFYLHS
20. Mak TW, Saunders ME, Jett BD, editors. *Primer to the immune response. 2nd ed*. Academic Cell; 2014. doi: 10.1016/C2009-0-62217-0 EDN: VEJPCD
21. Simon T, Kirk J, Dolezalova N, et al. The cholinergic anti-inflammatory pathway inhibits inflammation without lymphocyte relay. *Front Neurosci*. 2023;17:1125492. doi: 10.3389/fnins.2023.1125492 EDN: YFEFJO
22. Saitou M, Fujimoto K, Doi Y, et al. Occludin-deficient embryonic stem cells can differentiate into polarized epithelial cells bearing tight junctions. *J Cell Biol*. 1998;141(2):397–408. doi: 10.1083/jcb.141.2.397

23. Umeda K, Ikenouchi J, Katahira-Tayama S, et al. ZO-1 and ZO-2 independently determine where claudins are polymerized in tight-junction strand formation. *Cell*. 2006;126(4):741–754. doi: 10.1016/j.cell.2006.06.043
24. Saitou M, Furuse M, Sasaki H, et al. Complex phenotype of mice lacking occludin, a component of tight junction strands. *Mol Biol Cell*. 2000;11(12):4131–4142. doi: 10.1091/mbc.11.12.4131
25. Castro Dias M, Coisne C, Lazarevic I, et al. Claudin-3-deficient C57BL/6J mice display intact brain barriers. *Sci Rep*. 2019;9(1):203. doi: 10.1038/s41598-018-36731-3 Erratum in: *Sci Rep*. 2019;9(1):10702. doi: 10.1038/s41598-019-43511-0
26. Torices S, Daire L, Simon S, et al. Occludin: a gatekeeper of brain infection by HIV-1. *Fluids Barriers CNS*. 2023;20(1):73. doi: 10.1186/s12987-023-00476-7 EDN: DIHKGB
27. Sugiyama S, Sasaki T, Tanaka H, et al. The tight junction protein occludin modulates blood-brain barrier integrity and neurological function after ischemic stroke in mice. *Sci Rep*. 2023;13(1):2892. doi: 10.1038/s41598-023-29894-1 EDN: CMREJL
28. Kago T, Takagi N, Date I, et al. Cerebral ischemia enhances tyrosine phosphorylation of occludin in brain capillaries. *Biochem Biophys Res Commun*. 2006;339(4):1197–1203. doi: 10.1016/j.bbrc.2005.11.133
29. Wang W, Dentler WL, Borchardt RT. VEGF increases BMEC monolayer permeability by affecting occludin expression and tight junction assembly. *Am J Physiol Heart Circ Physiol*. 2001;280(1):H434–H440. doi: 10.1152/ajpheart.2001.280.1.H434
30. Elias I, Franckhauser S, Bosch F. New insights into adipose tissue VEGF-A actions in the control of obesity and insulin resistance. *Adipocyte*. 2013;2(2):109–112. doi: 10.4161/adip.22880
31. Bang S, Lee SR, Ko J, et al. A low permeability microfluidic blood-brain barrier platform with direct contact between perfusable vascular network and astrocytes. *Sci Rep*. 2017;7(1):8083. doi: 10.1038/s41598-017-07416-0 EDN: PSOYAI
32. Rahman A, Kefer J, Bando M, et al. E-selectin expression in human endothelial cells by TNF-α-induced oxidant generation and NF-κB activation. *Am J Physiol Lung Cell Mol Physiol*. 1998;275(3):L533–L544. doi: 10.1152/ajplung.1998.275.3.L533
33. Wyble CW, Hynes KL, Kuchibhotla J, et al. TNF-alpha and IL-1 upregulate membrane-bound and soluble E-selectin through a common pathway. *J Surg Res*. 1997;73(2):107–112. doi: 10.1006/jsre.1997.5207
34. Perez JA, Clinton SM, Turner CA, et al. A new role for FGF2 as an endogenous inhibitor of anxiety. *J Neurosci*. 2009;29(19):6379–6387. doi: 10.1523/JNEUROSCI.4829-08.2009
35. Tang MM, Lin WJ, Zhang JT, et al. Exogenous FGF2 reverses depressive-like behaviors and restores the suppressed FGF2-ERK1/2 signaling and the impaired hippocampal neurogenesis induced by neuroinflammation. *Brain Behav Immun*. 2017;66:322–331. doi: 10.1016/j.bbi.2017.05.013
36. Paton SEJ, Solano JL, Collignon A, et al. Environmental enrichment and physical exercise prevent stress-induced behavioral and blood-brain barrier alterations via Fgf2. *bioRxiv*. Preprint. 2023. doi: 10.1101/2023.11.08.566229
37. Tang MM, Lin WJ, Pan YQ, Li YC. Fibroblast growth factor 2 modulates hippocampal microglia activation in a neuroinflammation induced model of depression. *Front Cell Neurosci*. 2018;12:255. doi: 10.3389/fncel.2018.00255
38. Traina G. The role of mast cells in the gut and brain. *J Integr Neurosci*. 2021;20(1):185–196. doi: 10.31083/j.jin.2021.01.313 EDN: TGHZKS
39. Huang X, Lan Z, Hu Z. Role and mechanisms of mast cells in brain disorders. *Front Immunol*. 2024;15:1445867. doi: 10.3389/fimmu.2024.1445867 EDN: PUOWHX
40. Asahi M, Wang X, Mori T, et al. Effects of matrix metalloproteinase-9 gene knock-out on the proteolysis of blood-brain barrier and white matter components after cerebral ischemia. *J Neurosci*. 2001;21(19):7724–7732. doi: 10.1523/JNEUROSCI.21-19-07724.2001
41. Strbian D, Kovanen PT, Karjalainen-Lindsberg ML, et al. An emerging role of mast cells in cerebral ischemia and hemorrhage. *Ann Med*. 2009;41(6):438–450. doi: 10.1080/07853890902887303
42. Hu WW, Chen Z. Role of histamine and its receptors in cerebral ischemia. *ACS Chem Neurosci*. 2012;3(4):238–247. doi: 10.1021/cn200126p EDN: PMXUOF
43. Lambracht-Hall M, Konstantinidou AD, Theoharides TC. Serotonin release from rat brain mast cells in vitro. *Neuroscience*. 1990;39(1):199–207. doi: 10.1016/0306-4522(90)90233-t
44. Nautiyal KM, Dailey CA, Jahn JL, et al. Serotonin of mast cell origin contributes to hippocampal function. *Eur J Neurosci*. 2012;36(3):2347–2359. doi: 10.1111/j.1460-9568.2012.08138.x
45. Turkin A, Tuchina O, Klempin F. Microglia function on precursor Ccells in the adult hippocampus and their responsiveness to serotonin signaling. *Front Cell Dev Biol*. 2021;9:665739. doi: 10.3389/fcell.2021.665739 EDN: KXQFIC
46. Sidorova M, Kronenberg G, Matthes S, et al. Enduring effects of conditional brain serotonin knockdown, followed by recovery, on adult rat neurogenesis and behavior. *Cells*. 2021;10(11):3240. doi: 10.3390/cells10113240 EDN: LEDJFW
47. Perez-Dominguez M, Ávila-Muñoz E, Domínguez-Rivas E, Zepeda A. The detrimental effects of lipopolysaccharide-induced neuroinflammation on adult hippocampal neurogenesis depend on the duration of the pro-inflammatory response. *Neural Regen Res*. 2019;14(5):817–825. doi: 10.4103/1673-5374.249229
48. Leng F, Edison P. Neuroinflammation and microglial activation in Alzheimer disease: where do we go from here? *Nat Rev Neurol*. 2021;17(3):157–172. doi: 10.1038/s41582-020-00435-y EDN: CZJYEB
49. Isik S, Yeman Kiyak B, Akbayir R, et al. Microglia mediated neuroinflammation in Parkinson's disease. *Cells*. 2023;12(7):1012. doi: 10.3390/cells12071012 EDN: BBWEAD
50. Kurilova E, Sidorova M, Tuchina O. Single prolonged stress decreases the level of adult hippocampal neurogenesis in C57BL/6, but not in house mice. *Curr Issues Mol Biol*. 2023;45(1):524–537. doi: 10.3390/cimb45010035 EDN: KYZROU
51. Kurki SN, Srinivasan R, Laine J, et al. Acute neuroinflammation leads to disruption of neuronal chloride regulation and consequent hyperexcitability in the dentate gyrus. *Cell Rep*. 2023;42(11):113379. doi: 10.1016/j.celrep.2023.113379 EDN: ZLFOGY
52. Bröer S, Brookes N. Transfer of glutamine between astrocytes and neurons. *J Neurochem*. 2001;77(3):705–719. doi: 10.1046/j.1471-4159.2001.00322.x EDN: ETRNDL
53. Zou J, Wang YX, Dou FF, et al. Glutamine synthetase down-regulation reduces astrocyte protection against glutamate excitotoxicity to neurons. *Neurochem Int*. 2010;56(4):577–584. doi: 10.1016/j.neuint.2009.12.021
54. Sitcheran R, Gupta P, Fisher PB, Baldwin AS. Positive and negative regulation of EAAT2 by NF-kappaB: a role for N-myc in TNFalpha-controlled repression. *EMBO J*. 2005;24(3):510–520. doi: 10.1038/sj.emboj.7600555

ОБ АВТОРАХ

*** Тучина Оксана Павловна,** канд. биол. наук, доцент;
адрес: Россия, 236041, Калининград, ул. А. Невского, д. 14;
ORCID: 0000-0003-1480-1311;
eLibrary SPIN: 1916-6206;
e-mail: oktuchina@gmail.com

AUTHORS' INFO

*** Oksana P. Tuchina,** Cand. Sci. (Biology), Associate Professor;
address: 14 Nevskogo st, Kaliningrad, Russia, 236041;
ORCID: 0000-0003-1480-1311;
eLibrary SPIN: 1916-6206;
e-mail: oktuchina@gmail.com

Исмаилова Айназик Улукбековна;
ORCID: 0009-0002-5162-3884;
eLibrary SPIN: 9770-5930;
e-mail: ismailova.ainazikk@gmail.com

Ичеткина Ксения Владимировна;
ORCID: 0009-0004-8519-3354;
eLibrary SPIN: 3992-9830;
e-mail: ksenya.ichetkina@gmail.com

Шульц Маргарита Романовна;
ORCID: 0009-0000-0638-0911;
eLibrary SPIN: 3736-7801;
e-mail: margarita.r.schulz@gmail.com

Шульц Антон Сергеевич;
ORCID: 0009-0004-1844-554X;
eLibrary SPIN: 1828-7888;
e-mail: anton.s.schulz@gmail.com

Курилова Екатерина Александровна;
ORCID: 0000-0003-0031-116X;
eLibrary SPIN: 2724-1531;
e-mail: ekaterinakuuurilova@gmail.com

Ainazik U. Ismailova;
ORCID: 0009-0002-5162-3884;
eLibrary SPIN: 9770-5930;
e-mail: ismailova.ainazikk@gmail.com

Ksenia V. Ichetkina;
ORCID: 0009-0004-8519-3354;
eLibrary SPIN: 3992-9830;
e-mail: ksenya.ichetkina@gmail.com

Margarita R. Shults;
ORCID: 0009-0000-0638-0911;
eLibrary SPIN: 3736-7801;
e-mail: margarita.r.schulz@gmail.com

Anton S. Shults;
ORCID: 0009-0004-1844-554X;
eLibrary SPIN: 1828-7888;
e-mail: anton.s.schulz@gmail.com

Ekaterina A. Kurilova;
ORCID: 0000-0003-0031-116X;
eLibrary SPIN: 2724-1531;
e-mail: ekaterinakuuurilova@gmail.com

* Автор, ответственный за переписку / Corresponding author